Estimation of Additional Losses induced by Converters in Permanent Magnet Machines

by

Lucas Cueto Díaz

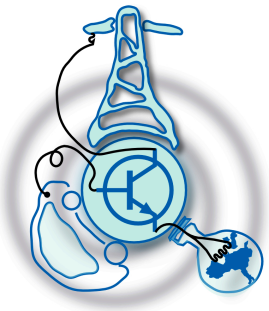

Submitted to the Department of Electrical Engineering, Electronics, Computers and Systems
in partial fulfillment of the requirements for the degree of
Erasmus Mundus Master Course in Sustainable Transportation and Electrical Power Systems
at the
UNIVERSIDAD DE OVIEDO
July 2014

Author .....

Certified by .....
Pablo García Fernández
Associate Professor
Thesis Supervisor

Certified by .....
Asier Rodríguez Díaz
Gamesa Generator Engineering Unit Manager
Thesis Supervisor

Estimation of Additional Losses induced by Converters in Permanent Magnet Machines

by

Lucas Cueto Díaz

Submitted to the Department of Electrical Engineering, Electronics, Computers and Systems
on July 26, 2014, in partial fulfillment of the
requirements for the degree of
Erasmus Mundus Master Course in Sustainable Transportation and Electrical Power Systems

Abstract

The scope of this Master Thesis is to develop a theoretic model in order to quantify and allocate the additional losses produced by the converter in a 5 MW Interior Permanent Magnet Machine (IPMSM). The modulation used by the converter, Space Vector Pulse Width Modulation (SVPWM), will contain high frequency harmonic voltages, that in interaction with the machine will cause the corresponding high frequency currents and thus a certain amount of additional losses in the stator windings.

This losses, depending on the machine design and operating point, can range from 1 to 20% of the total losses, and are usually neglected or estimated, but very rarely calculated. The main objectives of this Thesis aim to clarify the process of calculating that losses, and can be summed up in the following steps:

1. To design and validate a mathematical method to calculate the harmonic content of the supply voltages Vn and stator currents In, depending on converter and machine parameters, respectively.

2. To be able to introduce that harmonic content into a machine model that allows to calculate the additional losses from In.

3. To contrast that model with real data from the machine "G128", and to extend and generalize that model to other machines.

4. To develop a computer tool/model that allows to characterize that losses.

Thesis Supervisor: Pablo García Fernández
Title: Associate Professor

Thesis Supervisor: Asier Rodríguez Díaz
Title: Gamesa Generator Engineering Unit Manager

Acknowledgments

This thesis is part of the cooperation programme between Gamesa Electric and Universidad de Oviedo, and has been realized as an internal engineering project for Gamesa Electric.

The author of this thesis would like to offer special thanks the Electric Machines Design department, from Gamesa Electric, for all the help provided. Assistance from the Computational Electronics Department staff from University of Oviedo was greatly appreciated as well.

Contents

List of Figures

List of Tables

Chapter 1

Introduction

Within the scope of the industrial rotating machines, the progressive inclusion of PWM (Pulse Width Modulated) voltage converter based systems has become the norm in the present days. Rather than a sinusoidal waveform, these voltage converters present the peculiarity of generating rectangular voltage pulses with low rising time and variable pulse width. Feeding an electric machine with such a characteristic waveform is the cause of supplementary or additional losses in the stator of the aimed machine, being the main consequences: a) a decrease in the performance and b) an increased heating on the stator windings.

It is thereby necessary to have available an analytic calculus method for the estimation of the additional losses in the Permanent Magnet machines (those losses related to the high frequency harmonics coming from the converter and being therefore dependent on the modulation strategy). The quantification of that losses, due to the complex physics phenomena involved in them, becomes difficult, and there is no commonly accepted methods in the industry on such purpose. That is the reason why from the industry and University of Oviedo it has been detected the need of developing a mathematical model that is capable of characterizing such additional losses, which constitutes the origin of this project.

1.1 Stator Losses

The origin of the additional copper losses is related to the skin and proximity effects occurring in the stator windings when they are subjected to high frequency currents created by the modulation in the converter (in this case Space Vector Pulse Width Modulation). Each of the high harmonic currents will "see" an increased stator resistance at the harmonic frequencies where they occur: $m_f \pm 2kf_0$ and $2m_f \pm kf_0$, being m_f the switching frequency, f_0 the target output frequency and $k \in \mathbf{Z}$. This increment in the Ohmnic resistance at each of those frequencies will cause, even with low harmonic current amplitudes at that frequencies, a considerable amount of total power loss that needs to be added to the resistive losses calculated as I^2R, being I the nominal current and R the stator resistance at the nominal frequency and operating point temperature.

The effects of this circulating high frequency currents can be summed up within the following points:

- Overheating of winding conductors.
- Reduction in the overall efficiency.
- Increased electromagnetic noise in the machine.
- Increased torque ripple.
- Insulation damage in the windings.

1.2 State of the art

The first studies and derivation of the AC resistance equations in the machine windings was first presented in [4] and [13] . The analysis of the dependence of the stator resistance (and thus, the generation of additional copper losses) on the design parameters in industrial rotating machines is very well described in [14], with special scope in the induction machines (from the point of view of an stator, the calculations

still would have validity in the case of a permanent magnet machine). However, for the new permanent magnet machine designs, this phenomena has not been the main focus of the studies. Some studies can be found on this topic in [10] [9] [1]. Also several methods for the AC resistance in an inductor are discussed in [2] and [3], with special aim in the magnetic transformer design. However, as already commented, there is no general accepted method in the industry that covers the machines fed by a PWM converter, which means high frequency waveforms at their stator (PMSM, Induction machines) or rotor (DFIG).

1.3 Objectives of the Master Thesis

This Thesis is divided in three main stages:

1. **Stage 1. Characterization of the voltage harmonics.**
   In this first stage the study an analysis of the voltage harmonics present in the different types of modulation techniques that are used in the permanent magnet synchronous machines, with special interest in SVPWM and SPWM (sinusoidal PWM). This stage can be divided in:

   - Frequency Analysis of the voltage harmonics in the machine.
   - Contrast of the model obtained with real experimental data.

2. **Stage 2. Introduction of machine parameters. Study of the current harmonics.**
   In this stage some of the parameters of the machine are introduced in the model in order to be able to perform the analysis of the current harmonics. This stage can be divided in:

   - Introduction of the relevant parameters for the current study.
   - Frequency Analysis of the current harmonics of the machine.
   - Contrast of the obtained model with real experimental data.

3. **Stage 3. Introduction of the geometry of the machine and estimation of additional losses.**

   In this last stage of the project the rest of the parameters of the machine (winding geometry) will be included and the calculation and characterization of the additional losses of the machine produced by the converter will be performed.

   - Introduction of the relevant parameters for the calculation of the losses.
   - Calculation and characterization of the additional losses of the machine.
   - Contrast of the obtained model with real experimental data.
   - Development of the computer model/tool that allows to calculate the additional losses for the generalized case.

Chapter 2

SVPWM Modulation

2.1 Introduction to Space Vector PWM

In the conventional two-level full-bridge voltage source inverters (or 2-level VSI), a sinusoidal signal with varying amplitude and frequency is generated from a DC source. The load (in this case, a 3-phase IPMSM motor/generator) is connected between points a, b, and c. Depending on the status of the switches, the output terminals of each leg take the voltage values of $+\frac{V_{dc}}{2}$ or $-\frac{V_{dc}}{2}$ with respect to the center point of the DC source, N (see Fig. 2-1). The commutation sequence that governs the switches is imposed by a *modulation* process, that is responsible of synthesizing the output waveform.

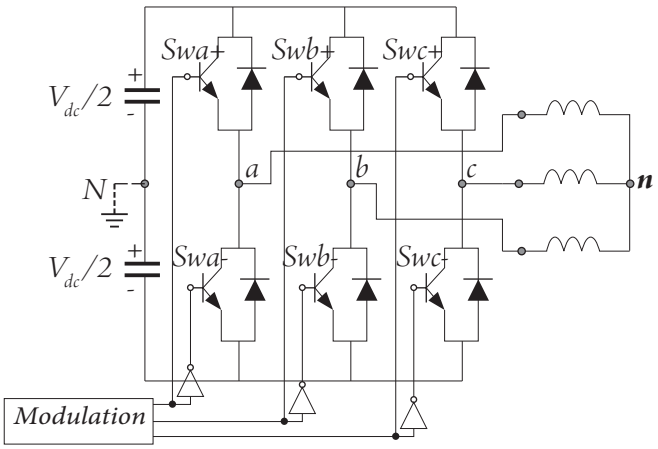

Figure 2-1: Two-level full-bridge three-phase VSI inverter.

The modulation technique applied to the inverter determines the use of the DC bus, the quality and linearity of the output voltage, the current ripple, the switching power losses, etc [5]. The switched operation of the electronic power converters has made possible to obtain high efficiency, high power density systems, being the *Pulse Width Modulation* (PWM) the basic technique to process the energy in these converters. The continuous improvements on the switching frequencies of the power transistors, and the increase on the computation capabilities of the DSPs, makes the research on modulation algorithms that are increasingly efficient and fast, to be a continuously evolving field.

The deep, microscopic study of the modulation process lead *Van der Broek*, in 1986, to propose an advanced modulation technique known as *Space Vector-Pulse Width Modulation* (SV-PWM) [19]. The interesting approach presented in this technique, its tight relation with the switching sequences experimented by the inverter, and its suitability to be applied in a DSP have contributed its extended use in industrial electronic applications. The results obtained with SV-PWM are identical to those resulting from the application of an older application technique, proposed by *King* in 1974 [11], that was based in the *addition of zero sequence signals* (ZSS-PWM). The analogic technique proposed by *King* came from a macroscopic analysis of the modulation process, focusing in extending the linear operation range of the inverter. Curiously, *King*'s contribution was not noticed by electrical/electronic engineers, perhaps due to the lack of clarity on its explanations. On the other hand, the elegance of the development proposed by *Van der Broek*, together with the emergence of the first low cost digital processors, lead SV-PWM to be considered as one of the most suitable modulation techniques for inverters with floating DC bus voltage (with respect to the neutral of the load).

The digital implementation of SV-PWM is based on the determination of the position of the reference voltage vector, the calculation of the time of application of each of the generating vectors, the choice of the correct sequence of those vectors, and the translation of those times into input references to the digital comparators that will finally generate the control signals of the inverter transistors.

2.2 Carrier Based PWM

2.2.1 Sinusoidal PWM

One of the most popular modulation methods that exist nowadays is the carrier-based PWM (CB-PWM) [7]. The simplest configuration of this modulation technique, *Sinusoidal PWM*, SPWM, obtains the switching signals of the inverter legs from the comparison between a reference voltage signal, that acts as a *modulating signal*, with another *carrier signal*, so that any time that the magnitude of the modulating signal is less or equal than the amplitude of the triangular carrier, there will exist a linear relation between the amplitude of the fundamental component of the output modulated voltage and the magnitude of that modulating signal, as shown in Fig. 2-2: In SPWM, the modulating signals form a three-phase balanced set that makes the

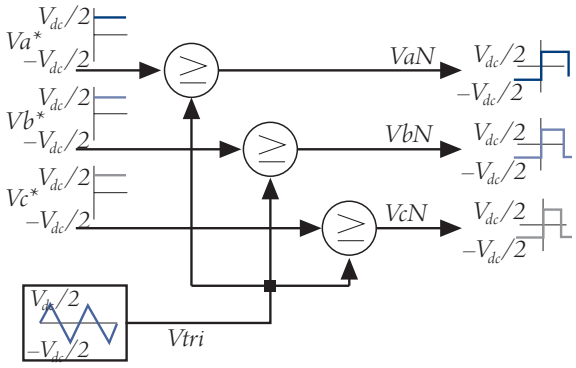

Figure 2-2: Carrier-based three-phase PWM modulation scheme.

amplitude, frequency and phase at the output of the inverter. The algebraic definition of the modulating signals of SPWM is presented in Eq. 2.1 to Eq. 2.3, where A is the maximum amplitude of the modulating signals and ω_m its angular frequency.

$$v_a^*(t) = A\sin(\omega_m t) \tag{2.1}$$

$$v_b^*(t) = A\sin(\omega_m t - \frac{2\pi}{3}) \tag{2.2}$$

$$v_c^*(t) = A\sin(\omega_m t - \frac{2\pi}{3}) \tag{2.3}$$

$$v_a^*(t) + v_b^*(t) + v_c^*(t) = 0 \tag{2.4}$$

The parameter that describes the relationship between reference and carrier is the *modulation index*, m, that is defined as the amplitude of the reference signal over the maximum amplitude of the carrier, that is, $V_{dc}/2$:

$$m = \frac{v^*_{Ph}}{V_{dc}/2} \tag{2.5}$$

where v^*_{ph} is the amplitude of the reference signal (modulating) for the phase-to-neutral voltage at the output of the inverter, and V_{dc} is the value of the DC bus voltage. When the inverter works in saturation, that means, when the inverter output voltage has a square waveform, the amplitude of the fundamental component of those square waveforms is the maximum output amplitude for a certain DC bus voltage. In that case, the inverter is working in 6-*step* mode, and there is another definition of modulation index, represented now by M:

$$M = \frac{v^*_{Ph}}{v_{6step}} \qquad v_{6step} = \frac{2}{\pi} \cdot V_{dc} \tag{2.6}$$

The *frequency modulation index*, N, shows the relation between the frequency of the carrier signal, f_c, with the frequency of the modulating signal, f_m:

$$N = \frac{f_a}{f_m} \tag{2.7}$$

When N is an integer value, the modulation is *synchronous*, suitable to applications that require a low modulation index ($N < 21$). When N is not an integer, the modulation is *asynchronous*; characterized for generating non-periodic voltage pulses at the output. The synchronization has importance in high power applications, where low carrier frequencies are required in order to reduce switching losses. In such applications, the harmonic content of the asyncrhonous modulation is higher than in the synchronous modulation.

Regarding the value of M, it is possible to differentiate between two modes of operation of the PWM modulation: linear and non-linear. In the linear operation, the peak of the modulating signal is lower or equal than the peak of the carrier signal

($M <= 1$). In the non linear mode, amplitude of the modulating signal is greater than the amplitude of the carrier ($M > 1$). As shown in Fig. 2-3, when the amplitude of the reference voltage v_a^* exceeds the level $V_{dc}/2$, the intersections between the carrier and the modulating signal no longer take place, and the generated pulses in the comparison remain in a constant level. In general terms, SPWM is a simple technique that

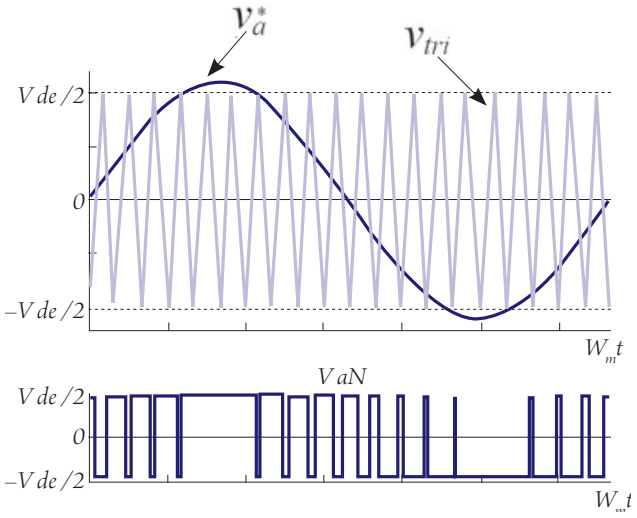

Figure 2-3: Overmodulation of the phase a in SPWM.

guarantees good results in all working conditions, including overmodulation range, and that presents a good harmonic performance. This good characteristic is due to its constant switching frequency, that generates a defined spectrum, with high-frequency components and low-order harmonic reduction. For that reasons, the first versions of this method were greatly appreciated by the industry, but soon it was evidenced that *the limitation in their linear range made the motors to operate with lower voltages than the nominal ones, therefore reducing efficiency and performance.* The modulation linear range can be expressed as the maximum modulation index inside the linear zone, in the case of SPWM this is equal to $m_{max,linear} = 1$. Fig 2-4 shows the linear range for SPWM.

2.2.2 Zero Sequence Signal PWM

The inverters in which the middle point of the DC bus, node '0'. is floating with respect to the neutral point of the system connected to the output of the inverter,

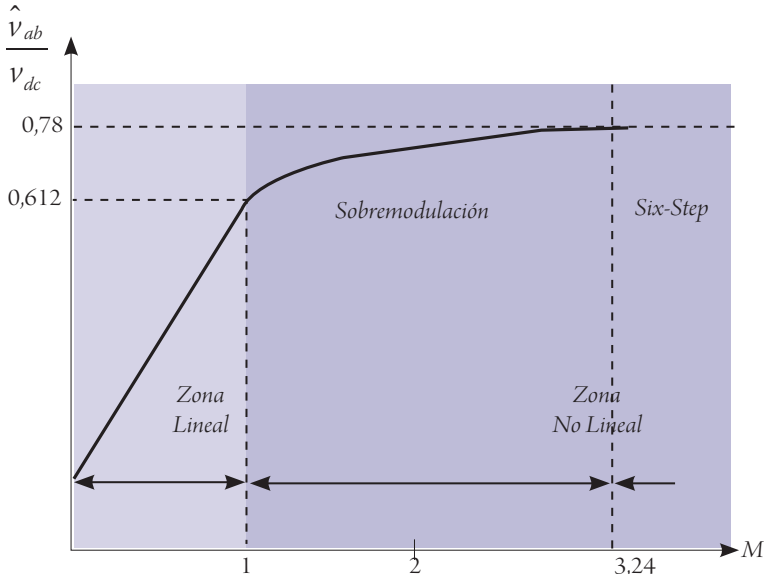

Figure 2-4: Characteristic curve of SPWM. Relation between the modulation index and the percentage of utilization of DC bus.

node 'n', that is, the TLFB and FLFB inverters, present an additional degree of freedom consisting on the regulation of the floating voltage of that bus, v_{0n}. The exploitation of that degree of freedom brings the appearance of a new category in the modulation techniques of the inverter. Following Fig. 2-5, these techniques are based on the modification of the original voltage references by means of the addition of a zero sequence signal (ZSS PWM), and constitute the second great contribution to the PWM modulation. In ZSS-PWM, the zero sequence signal added to the original

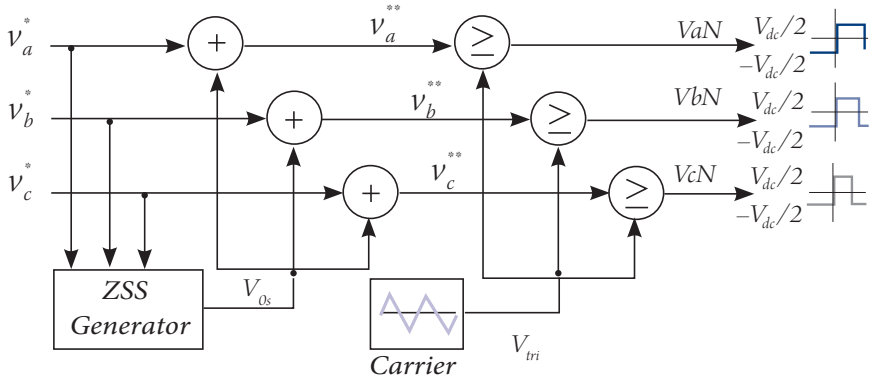

Figure 2-5: Zero Sequence Signal PWM modulation process.

references will be reflected spontaneously, and sign changed, into the floating voltage

of the DC bus. Considering the fact that the objective of the PWM modulation is to achieve that the information of the amplitude of the reference signal is contained in the mean value of the train of pulses generated, the phase to neutral voltages can be written as shown in Eq. 2.8 to 2.10, in which it is noticeable the influence of the zero sequence signal over the phase voltages. Note that in the line-to-line voltages (Equation 2.11 to 2.13), v_{0s} has disappeared, confirming its non-existing influence over the shape of the line-to-line voltages (this is the reason why this signal is called *zero* signal).

$$v_{aN}(t) = A\sin(\omega_m t) + v_{0s}(t) \tag{2.8}$$

$$v_{bN}(t) = A\sin(\omega_m t - \frac{2\pi}{3}) + v_{0s}(t) \tag{2.9}$$

$$v_{cN}(t) = A\sin(\omega_m t - \frac{4\pi}{3}) + v_{0s}(t) \tag{2.10}$$

$$v_{ab}(t) = A\sqrt{3}\sin(\omega_m t + \frac{\pi}{6}) \tag{2.11}$$

$$v_{bc}(t) = A\sqrt{3}\sin(\omega_m t - \frac{3\pi}{2}) \tag{2.12}$$

$$v_{ca}(t) = A\sqrt{3}\sin(\omega_m t - \frac{5\pi}{6}) \tag{2.13}$$

Adding the signals defined in Eq. 2.8 to 2.10 and considering that the sum of three-phase sinusoidal signals are zero, the v_{0s} signal can be formulated in terms of the modulating signals v_i^{**} as shown in Eq. 2.14:

$$v_{0s}(t) = \frac{1}{3}(v_a^{**}(t) + v_b^{**}(t) + v_c^{**}(t)) \tag{2.14}$$

In this technique, by means of properly selecting the zero sequence signal, the linear range of the inverter can be extended up to the value $m_{max,lin} = 2/\sqrt{3} = 1,1547$ (reflected in Fig. 2-6). In this sense, the addition of a sinusoidal signal of amplitude 1/6 and triple frequency (*Triplen Harmonic Injection PWM*-THIPWM 1/6) results in the linear range extended up to that value. If the amplitude of the added tripled frequency signal is of 1/4 of the sinusoidal reference signal (THIPWM 1/4), the

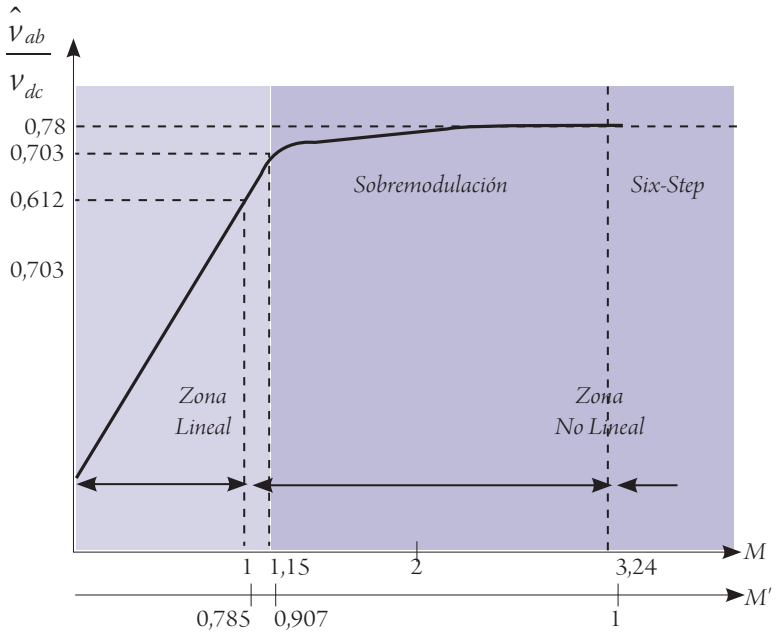

Figure 2-6: Characteristic curve of SVPWM and other methods PWM of maximum linear range.

linear range is a bit reduced $m_{max,lin} = 1,117$, but the harmonic content of the output current of the inverter is minimum. These two THIPWM modulators present certain complexity in the implementation, as much as the calculation of the tripled frequency signal involves high computational requirements, and thus its popularity has not reached the industrial scope and only endures in the academic ambit [8]. The addition of a triangular signal with a peak value equal to 1/4 of the sinusoidal reference signal and triple frequency (*Carrier-Based Space Vector PWM* or CB-SVPWM) also applies in order to obtain the maximum value of the linear range of the inverter, and offers optimum results regarding the current ripple, which makes it a powerful technique to be used in industrial applications. This modulation process offers the same results as the ones obtained when using the vector modulation with symmetrical distribution of the zero-vectors (this scheme is explained in the next section), hence its acronym [20].

The comparison between Carrier Based SVPWM and Sinusoidal PWM line-to neutral reference voltages is presented in Fig. 2-8, showing that the resulting line-to-line voltages commands are exactly the same.

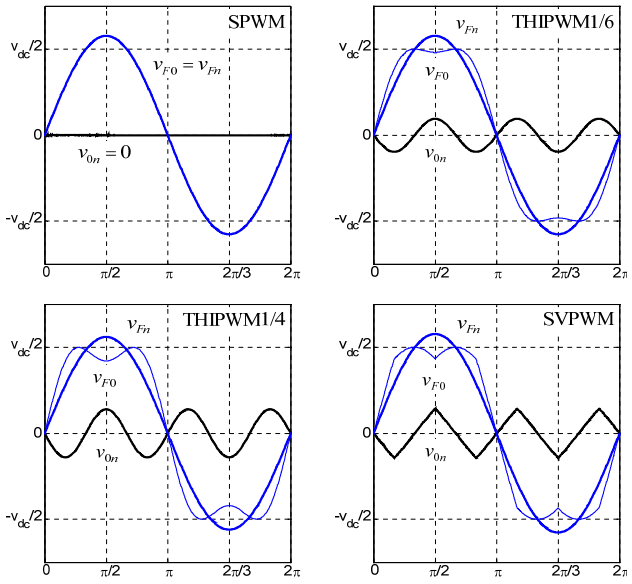

Figure 2-7: Different continuous PWM waveforms for m=1.154.

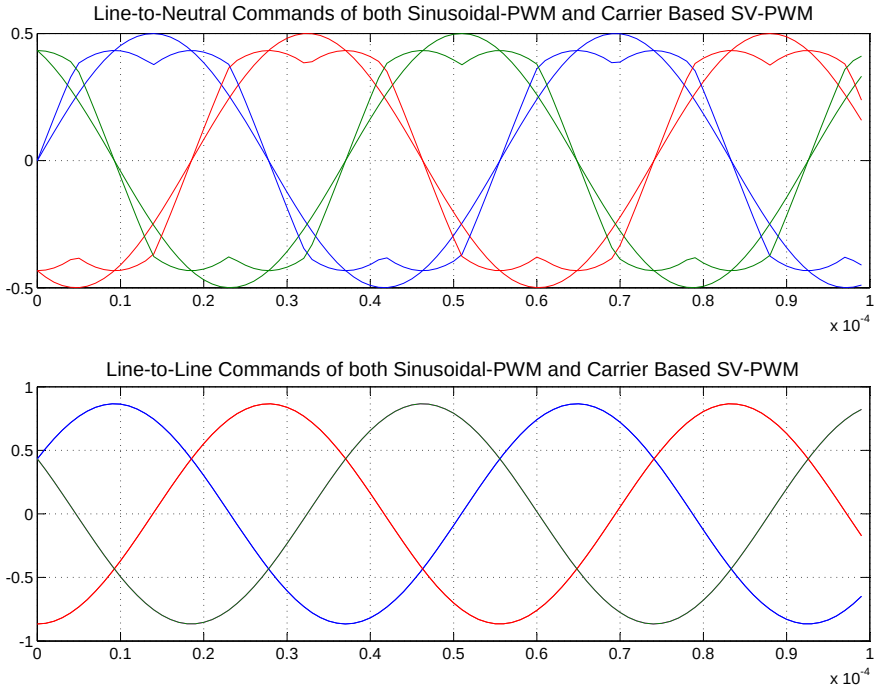

Figure 2-8: Comparison between Carrier Based SVPWM and Sinusoidal PWM line-to-neutral and line-to-line reference voltages

2.3 Space Vector PWM

This approach implies the synthesis of a reference space vector V^* in the plane $\alpha\beta$ by means of the instantaneous application of one the eight possible states of a VSI.

The 8 spatial voltage vectors that is possible to create in a three-phase two-level VSI

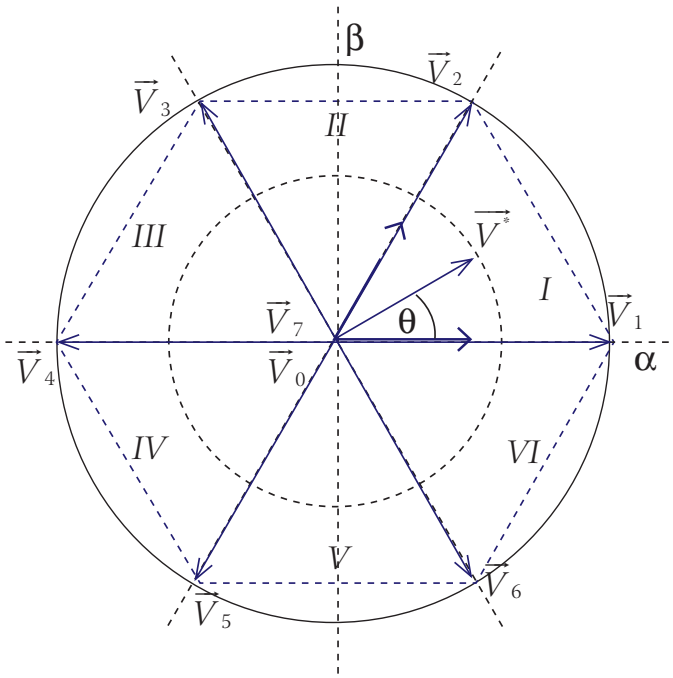

Figure 2-9: SVPWM Hexagon of Inverter Voltages.

may be classified in two groups: active vectors $V_1 - V_6$ and zero vectors V_0 and V_7; they are illustrated in Fig. 2-9. All the active vectors have the same magnitude and are phase shifted by 60°, therefore, they can be expressed by means of Eq. 2.15:

$$V_i = \frac{2}{3} \cdot V_{dc}\, e^{\frac{j(i-1)}{3}} \tag{2.15}$$

in which $i = 1, 2...6$ is one of the sectors of the hexagon in which the space is divided by the six active vectors. In a three-level inverter with the DC bus isolated with respect to the neutral point of the system, the floating DC bus voltage is equal to:

$$v_{Nn} = -\frac{1}{3}\left(v_{aN} + v_{bN} + v_{cN}\right) \tag{2.16}$$

Table 2.1: Inverter Voltages normalized with respect to $v_{dc}/2$

State	**Vector**	v_{aN}	v_{bN}	v_{cN}	v_{Nn}	v_{an}	v_{bn}	v_{cn}
111	$\vec{V_0}$	1	1	1	-1	0	0	0
100	$\vec{V_1}$	1	-1	-1	1/3	4/3	-2/3	-2/3
110	$\vec{V_2}$	1	1	-1	-1/3	2/3	2/3	-4/3
010	$\vec{V_3}$	-1	1	-1	1/3	-2/3	4/3	-2/3
011	$\vec{V_4}$	-1	1	1	-1/3	-4/3	2/3	2/3
001	$\vec{V_5}$	-1	-1	1	1/3	-2/3	-2/3	4/3
101	$\vec{V_6}$	1	-1	1	-1/3	2/3	-4/3	2/3
000	$\vec{V_7}$	-1	-1	-1	1	0	0	0

This means that the inverter output voltages v_{an}, v_{bn}, v_{cn}, can be calculated as:

$$v_{an} = v_{aN} + v_{Nn} \tag{2.17}$$

$$v_{bn} = v_{bN} + v_{Nn} \tag{2.18}$$

$$v_{cn} = v_{cN} + v_{Nn} \tag{2.19}$$

The leg voltages corresponding to all possible switching states of the inverter are presented in Table 2.1. Note that the homopolar component of the output inverter voltages is zero for all switching states:

$$v_{aN} + v_{bN} + v_{cN} = 0 \tag{2.20}$$

The reference voltage V^* follows the equation:

$$\vec{V}^*(t) = m\frac{V_{dc}}{2}\ e^{j2\pi f_n t} = m\frac{V_{dc}}{2}\ e^{j\omega_n t} \tag{2.21}$$

where m, the modulation index, is defined for SVPWM as:

$$m = \frac{V_{L-Lpeak}}{V_{dc}} \tag{2.22}$$

Any reference voltage inside of the limits of the hexagon can be synthesized,in each switching period, by means of its de-composition in the two adjacent active vectors

and the addition of the zero-vectors. Consider that the reference voltage is located in Sector I, following the Volt-Second Balance principle, the average output voltage vector can be expressed as [8]:

$$\vec{V}^* = \frac{t_1}{T_s}\vec{V_1} + \frac{t_2}{T_s}\vec{V_2} \tag{2.23}$$

where T_s is the switching period.

Operating the modulus of the two vector terms in Eq. 2.23, the application times of the vectors $\vec{V_1}$ and$\vec{V_2}$ are obtained:

$$t_1 = \frac{\sqrt{2}\left|\vec{V}^*\right|}{v_{dc}} T_s \sin\left(\frac{\pi}{3} - \theta\right) \tag{2.24}$$

$$t_2 = \frac{\sqrt{2}\left|\vec{V}^*\right|}{v_{dc}} T_s \sin\left(\frac{\pi}{3}\right) \tag{2.25}$$

where θ is the relative angle of rotation of the reference vector in the scoped sector. As long as the reference vector is inside the hexagon shown in Fig. 2-9, the following relationship must be accomplished:

$$t_1 + t_2 \leq T_s \tag{2.26}$$

The residual time until the total duration of the switching period is reached is reserved to the application of the zero vectors V_0 and V_7. The philosophy acknowledged in the equations 2.24 and 2.25 is identical in all the variants of SV-PWM. The only difference among the different techniques lies in the the technique used when arranging the duration and allocation of the zero vectors [6]. However, for all cases it must be satisfied that:

$$t_{0,7} = t_0 + t_7 = T_s - t_1 - t_2 \tag{2.27}$$

The different strategies used to determine the duration of the two zero vectors are intrinsically linked with the techniques used in the ZSS-PWM modulation. In fact, as evinced in Eq. 2.23, the allocation of the zero vectors does not affect the voltage vector

synthesized at the inverter output, modifying only the value of the DC bus floating voltage. Each of the techniques will lead to a different composition of the output voltage harmonics and switching losses. The objective is to reduce switching losses (number of commutations per period) and THD of the output voltage. There are several methods suggested in the literature for arrangement of states in a fundamental period; however, the most popular ones are:

- Symmetrical placement of both zero vectors along the fundamental period, which receives the name of *conventional SV-PWM*.
- Elimination of one zero-vector in each cycle (reducing switching losses), which receives the name of *discontinuous SV-PWM* or *bus-clamped*.

The selected method for the realization of the simulations and calculations is the *conventional SV-PWM*, for being the most widely used in industry and the one applied in the test bench where measures are taken. The zero-vector times in this case are directly obtained by symmetry:

$$t_0 = t_7 = \frac{T_s - t_1 - t_2}{2} \tag{2.28}$$

The next section analyzes the harmonic performances of the different PWM methods.

2.4 Harmonic Performance

The Total Harmonic Distortion THD reflects the energy of the waveform content and it is defined as:

$$\text{THD} = \frac{\sqrt{\sum_{h-2}^{n} V_h^2}}{V_1} \tag{2.29}$$

where V_1 is the rms value of the fundamental component of the voltage and V_h is the rms value of the h^{th} harmonic.

The analysis of the different techniques (Sinusoidal PWM for two and three-level inverters, and SV-PWM using conventional and discontinuous placement of zero vec-

tors) is performed using $V_{dc} = 1050$V, $V_{LLrms} = 600$V, $f_n = 89.6$ Hz, and $f_{sw} = 5000$ Hz, yielding modulation index $m = 0.808$ and frequency index $n = 55.8$. The results obtained are shown in Figs. 2-10 and 2-11.

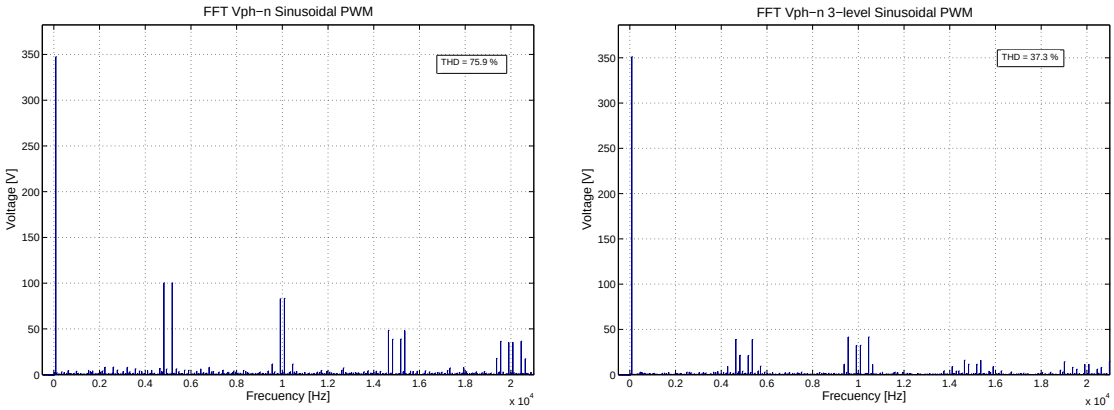

Figure 2-10: Harmonic spectrum of phase-to-neutral voltages of SPWM for two and three level inverters.

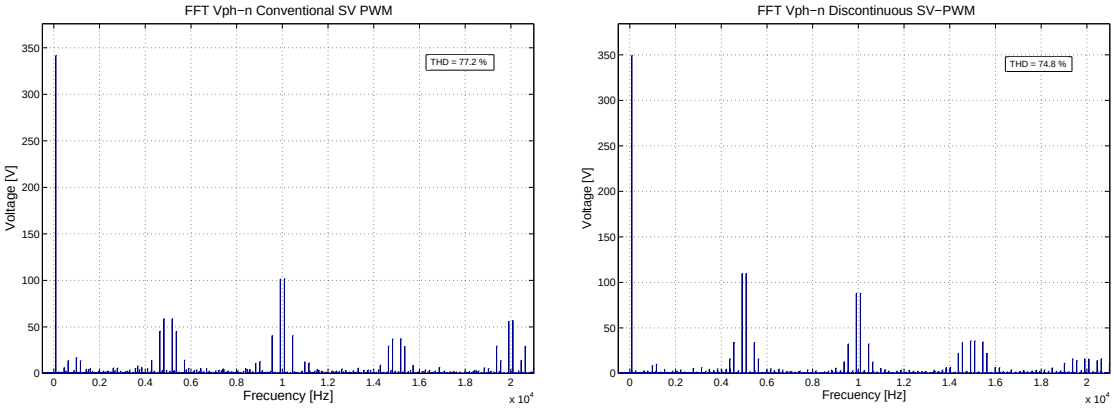

Figure 2-11: Harmonic spectrum of phase-to-neutral voltages of SV-PWM for conventional and discontinuous placement of zero-vectors.

The results show that, excluding 3-level SPWM, all of them have similar THD in the voltage waveforms, even though the distribution of the lateral bands around the switching frequencies is quite different. The summary about the harmonic contents of these different types of modulation is provided in Table 2.2.

Table 2.2: Harmonic decomposition of V_{ph-n} for S-PWM and SV-PWM. $m = 0.808$ and $n = 55.8$.

Harmonic	**Conventional SV-PWM**	**Discontinuous SV-PWM**	**Two-level SPWM**	**Three-level SPWM**
f_n	100	100	100	100
f_{sw}-$4f_n$	13.24	9.71	1.88	11.04
f_{sw}-$2f_n$	17.14	31.51	28.7	6.07
f_{sw}+$2f_n$	17.18	31.49	28.7	6.03
f_{sw}+$4f_n$	13.2	9.72	1.80	11.06
$2f_{sw}$-$7f_n$	0.28	3.63	1.12	3.24
$2f_{sw}$-$5f_n$	11.8	9.21	3.33	11.84
$2f_{sw}$-f_n	29.6	25.23	23.87	9.19
$2f_{sw}$+f_n	29.8	25.23	23.98	9.23
$2f_{sw}$+$5f_n$	11.8	9.20	3.33	11.85
$2f_{sw}$+$7f_n$	0.33	3.58	1.14	3.18
THD (%)	**77.2**	**74.8**	**75.9**	**37.3**

Chapter 3

Wind Power IPMSM Generator

3.1 Modular System Layout

The machine subject of study is the three-phase 5 MW A-kind Generator (Fig. 3-1), that is intended to work both in on-shore and off-shore configurations.

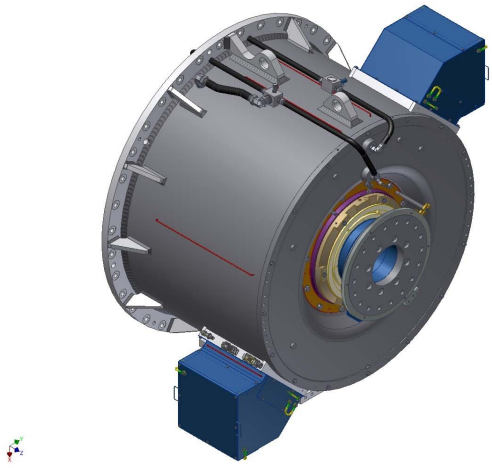

Figure 3-1: 3D mechanical model of the A-type IPMSM

It is an interior permanent magnet synchronous generator with a modular design configuration: its stator its divided in six sets of three-phase windings (multi-winding layout). All the theory explained before is perfectly valid in this new breed of machines; the only difference is that each of the winding sets, or *module*, has its own neutral wire, so there are 6 different stator circuits. Each of the modules forms 4

consecutive poles (conforming a total of 24 poles).

Each set of windings is fed by an individual back to back three-phase converter, making a total of six converters that share the full power of the generator (see Fig. 3-1). The output of these is parallel connected, forming a LV three-phase system. Before sending this power to the electrical substation, a LV/MV transformer is needed in order to step up the voltage and reduce the current ratings (and Joule losses) of the cables. This transformer is located in the tower to minimize losses, usually in a chamber under the nacelle.

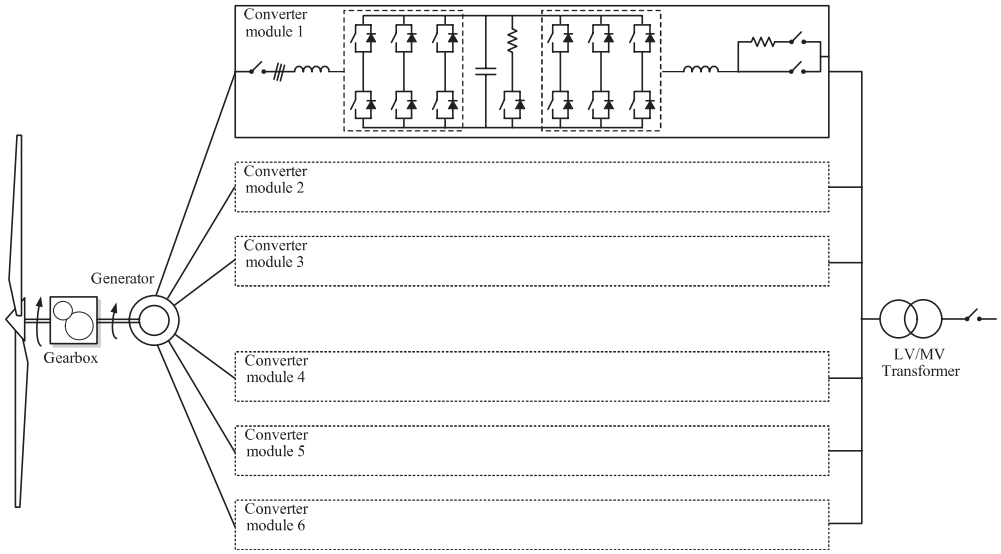

Figure 3-2: Modular configuration of the IPMSM

With this design the reliability of the system is increased dramatically: the machine is able to keep operation even if only two of the stator modules remain active (although the power produced would be reduced to 2/6 of the total power). This capability is strongly appreciated in comparison to older designs where very often a single switching device failure in the power converter was translated in the whole turbine to shut down until the component was replaced. Other advantages of this topology over other configurations (DFIG,PMSM with single full-power converter), apart from the increased reliability of the system, can be listed as:

- Switching devices such as IGBTs are less likely to fail since they handle a fraction of the total current.

- The overall electrical efficiency (power converter + electric machine) is increased, as the current handled by the switches is lower.
- The power quality at the grid side is higher, as harmonic distortion can be reduced by means of interleaving (phase-shifting) techniques.
- The passive filters used both in machine and in grid side are reduced in size.
- This configuration can potentially remove the LV/MV transformer if the converters' grid side is connected in series.

As one can expect from Fig. 3-2 the converters must be synchronized both in grid side and in machine side: The voltage and current waveforms at both sides of each of the converters are expected to be the same (usually interleaving or phase-shifting techniques are used at the grid side to improve power quality). Between converter and machine it is included a dv/dt filter and an L filter in order to prevent the windings from short circuits.

3.2 AC Winding Design

The permanent magnet synchronous machine consists in a magnetic circuit and an electric circuit. The *magnetic circuit* consists on a rotating inductor, or rotor, and a static induced, or stator. The *rotor* consists of a set of magnets (that inherently create the rotating magnetic flux) placed on a ferromagnetic core , that has high magnetic permeability, formed by thin steel alloy sheets placed in the axial direction , like in the conventional asynchronous machines. This ferromagnetic material will contain the closed flux paths that start and end in the north and south poles of the magnets. The reason why this core is formed by laminated magnetic sheets is to reduce Foucault (parasitic) currents. There are many possible configurations for the placement of the magnets in the rotor (surface, inset, interior) that are not discussed here as it is not our subject of study. It is enough to know that the scoped machine is an interior magnet kind.

The *stator* consists of an integration of packages of magnetic sheets in which it is possible to distinguish between 2 parts: the *yoke* is the external cylindrical part, from which interior surface come out the *teeth*. In between these teeth lay the gaps that are called *slots*. This magnetic set is also called the *armature*, and it is fixed by means of screws, bolts or threaded rods to an external smelted steel part called *frame*, that acts as the mechanic support of the stator.

The induced *electric circuit* is formed by the coils located in the slots of the stator armature. The length of the copper that takes part in the energy-conversion process is called conductor, or active part of the set of stator windings, and is located in the axial slots. The non-active part of the windings is located at the end-windings or outside the slots. In the AC machines, the windings are open at certain points of the end of the windings to form the poles of the machine in two or more parallel circuits.

3.2.1 Configuration of AC stator windings

The configuration of the stator windings is one of the key points in the design of the rotating machine, and it is of crucial importance for the calculation of copper losses and additional copper losses [16] [15]. The main two types of windings are *concentric windings* and *distributed windings*. In the concentrated kind, all the winding turns are wound together in series to form one multi-turn coil, and all the turns have the same magnetic axis (see Fig. 3-3).

In the distributed kind, all the winding turns are arranged in several full-pitch or fractional-pitch coils, that are then housed in the slots and spread around the air-gap periphery to form phase windings. Among the distributed kind, it is possible to distinguish between *lap* and *wave* windings (see Fig. 3-4). All AC windings must verify the following characteristics:

- All phases must have the same number of turns in series
- In windings with parallel circuits all paths must have the same resistance and produce identical emfs, both in frequency and amplitude.

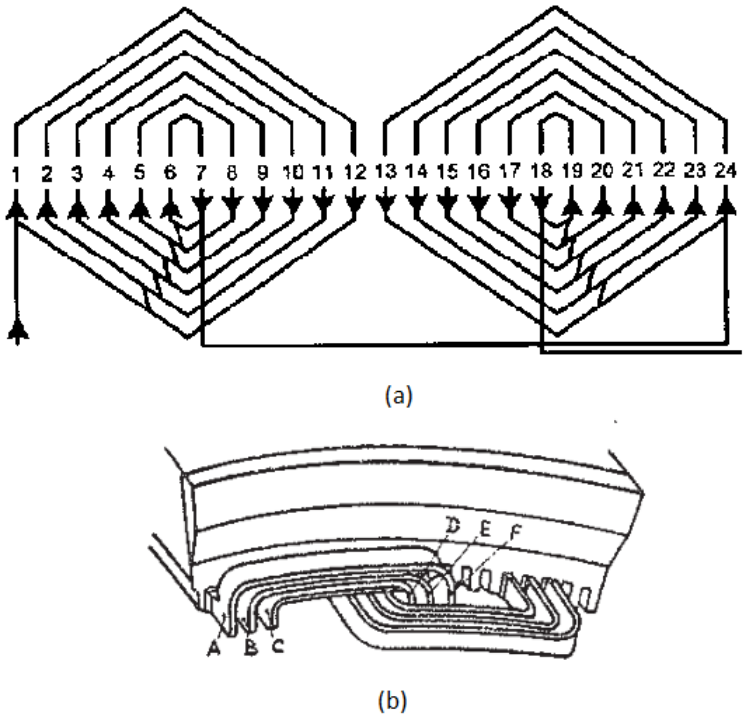

Figure 3-3: Two consecutive poles of a single-phase concentric winding: a)One-phase diagram b)End-winding

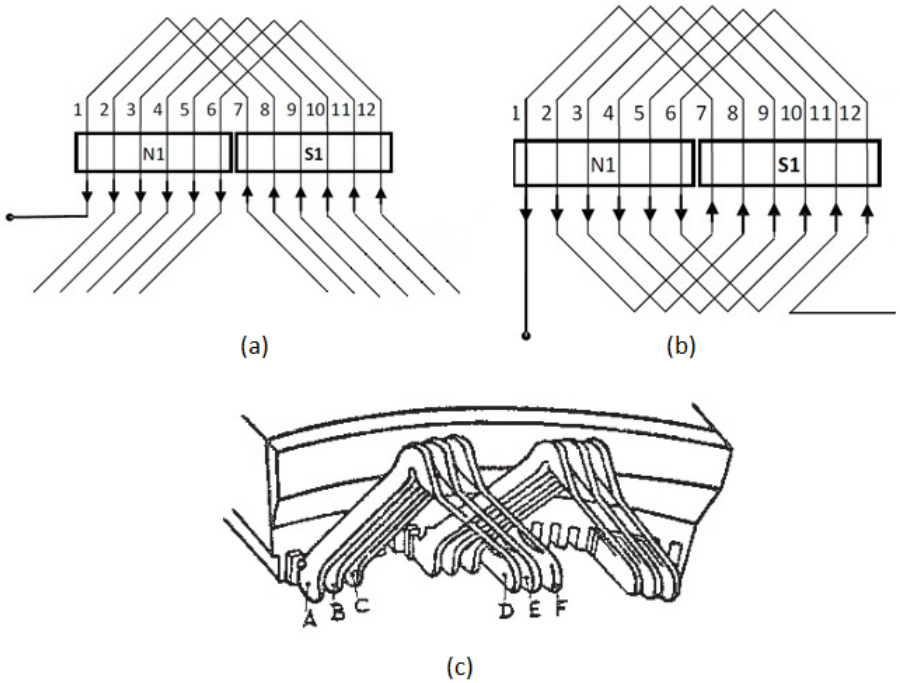

Figure 3-4: Two consecutive poles of single-phase distributed winding: a) Wave winding b) Lap winding c) Lap end-winding

- The phases must have a phase shift equal to that of the characteristic electrical angle of the power system (in the case of a 3-phase winding, the angle will be 120°).

The slot pitch τ_u and the slot angle α_u are the core parameters of the slot winding. The slot pitch is measured in metres, whereas the slot angle is measured in electrical degrees. The number of slots being Q and the diameter of the air gap D, we may write

$$\tau_u = \frac{\pi D}{Q}; \qquad \alpha_u = p\frac{2\pi}{Q} \tag{3.1}$$

The pole pitch is defined as the peripheral distance between identical points of two adjacent poles. It is always equal to 180 electrical degrees. However, the coil-pitch Y_k, or the distance between the two coil-sides of a coil, is not always equal to the pole pitch, being sometimes shortened or *chorded* (see Fig. 3-5) in order to lower the amount of copper needed in the end windings, and also to improve the emf produced.

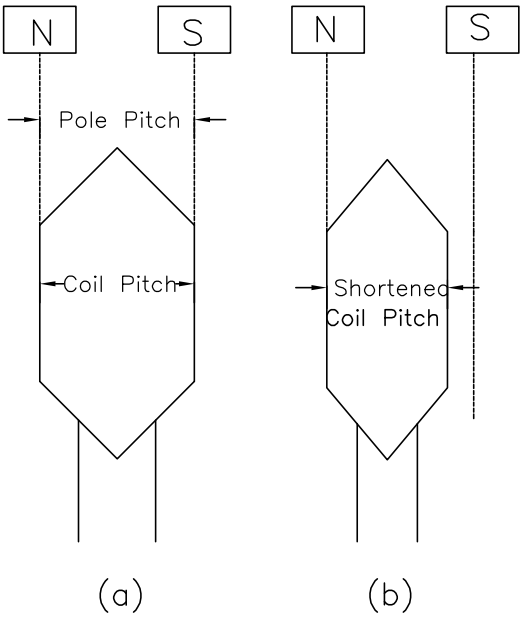

Figure 3-5: One coil of the winding a) Full-pitch Winding b) Chorded Winding

It should be noted that, in real world, most windings are not full-pitched nor concentrated [12]. Fortunately, these shortcomings can be accommodated by the use of *winding factors*. The simplest definition of a winding factor is the ratio of flux

λ [Wb] linked by an actual winding to the flux that would have been linked by a full-pitch, concentrated winding with the same number of turns. That is:

$$k_w = \frac{\lambda_{actual}}{\lambda_{full-pitch}} \tag{3.2}$$

A polar group is defined as the coils of the same phase that, connected in series, correspond to the same pole. The polar groups are then connected between them in series or in parallel, forming identical branches, to build up an entire phase of the windings. Depending on the way of connecting the polar groups of each phase, it is possible to classify the windings on: *per pole windings*, in which there are as many polar groups per phase, G_{ph}, as poles, $2p$, has the electric machine:

$$G_{ph} = 2p \tag{3.3}$$

; or *per consecutive pole windings*, in which the number of polar groups per phase, G_{ph}, is equal to the number or pole pairs of the machine:

$$G_{ph} = p \tag{3.4}$$

Fig. 3-6 shows the differences between them. In practice, most of the windings are executed *per pole*, except the concentric three phase windings, that are executed *per consecutive pole*. The polar groups are also defined by the parameter *number of slots per pole and phase*, q. If p is the number of pole pairs and m the number of phases, then:

$$q = \frac{Q}{2pm} \tag{3.5}$$

If q is an integer number, it is the case of an *integral slot* winding. On the contrary, if q is not an integer, then the winding is a *fractional slot* type.

As commented in the previous paragraph,the polar groups that form one phase can be connected between them in series, using the two techniques mentioned, or

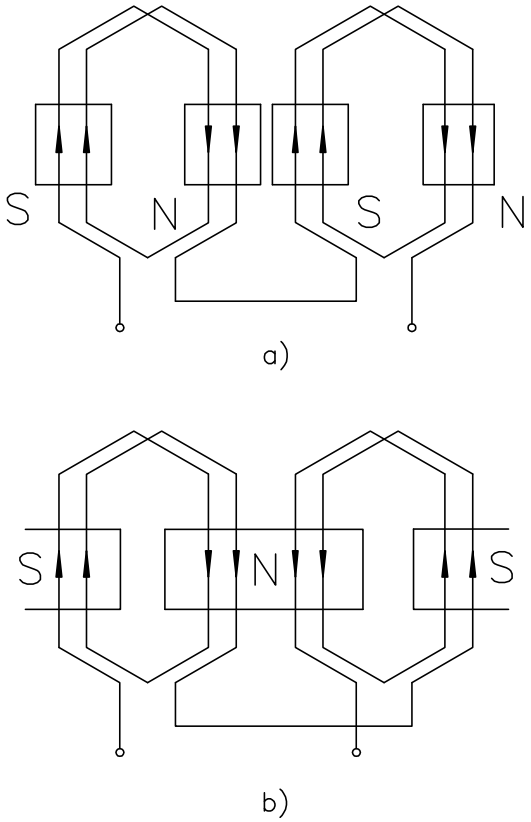

Figure 3-6: Two different types of pole group connections: a) per pole b) per consecutive pole

in parallel. All the parallel branches of a phase must be identical, so that the emf induced in them is the same and they have the same impedance. Being N_{ph} the total number of turns of one phase and a the number of parallel branches of that phase, then each of the branches will have N turns connected in series:

$$N = \frac{N_{ph}}{a} \tag{3.6}$$

If the total current that flows through one phase is I, the current that flows through each branch is equal to:

$$I_{br} = \frac{I}{a} \tag{3.7}$$

Note that the number of parallel branches that can be used in a lap winding is conditioned by the number of polar groups of the machine (the number of parallel branches must be an integer divisor of the number of polar groups per phase). A winding of b coils per pole pair and phase has $p * b$ coils per phase. If each of these

coils has N_r turns in series, this winding satisfies the following relationships:

$$N_{ph} = pbN_r \quad \text{turns per coil} \tag{3.8}$$

$$N = \frac{pbN_r}{a} \quad \text{turns per parallel branch} \tag{3.9}$$

$$B = mpb \quad \text{total number of coils, including the three phases} \tag{3.10}$$

Another classification of the windings is made taking into account the number of coils per slot: therefore it is possible to talk about single layer winding or double layer winding. In a single layer winding, each slot has one active side of a coil, so the following relationship is accomplished (Q is the total number of slots):

$$Q = 2B \tag{3.11}$$

Whereas in the double layer winding, there are two active sides per slot:

$$Q = B \tag{3.12}$$

Fig. 3-7 illustrates the shape of a double layer lap winding:

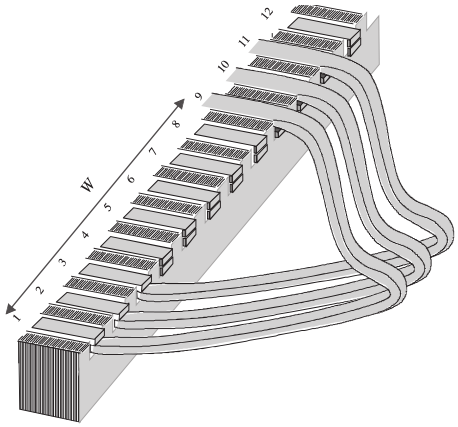

Figure 3-7: Double Layer Lap Winding

The advantages of adding a double layer over only considering one single layer can be listed as []:

- Easier to manufacture and lower cost of the coils

- Fractional-slot winding can be used
- Chorded-winding is possible
- Lower leakage-reactance and thus better performance of the machine
- Better emf waveform for generators.

The modern IPMSM in the range of 2.5 to 10 MW use *chorded, integral slot, double layer lap winding*, so the study of the losses in centered in this type of windings. They are designed to work in low voltages (690 V L-L) and high currents (1000 - 2000 A), so the isolation between layers do not need to be as demanding as in other higher voltage machines.

However, the high currents demand a larger coil section, and will produce more copper losses. This is the reason why the coils are not formed as a single thick conductor, but several conductors that can be connected, in the same coil, in series or in parallel, and share the current between the beginning and the end of the coil. This technique reduces the skin and proximity effects, and thus the additional copper losses of the machine. Note that different types of wire can be used for the winding of an AC machine: they can be classified as *form-wound* if they use rectangular straps, or *random-wound* if they are formed by round wires. Usually for the high current range the form-wound type is preferred, while the random-wound machines are used in medium-low current motors. Fig. 3-8 shows the inside shape of these two types of configurations.

3.2.2 Electromagnetic Behaviour of AC Windings

The fundamental air-gap single-phase mmf [measured in *Amperes-turn*, [A t]] wave of a distributed multi-pole winding is:

$$\mathcal{F}_{ph} = \frac{4}{\pi} \frac{k_w N_{ph}}{2p} \cdot I_{ph} \cdot \cos\left(p\theta_{ph}\right) \tag{3.13}$$

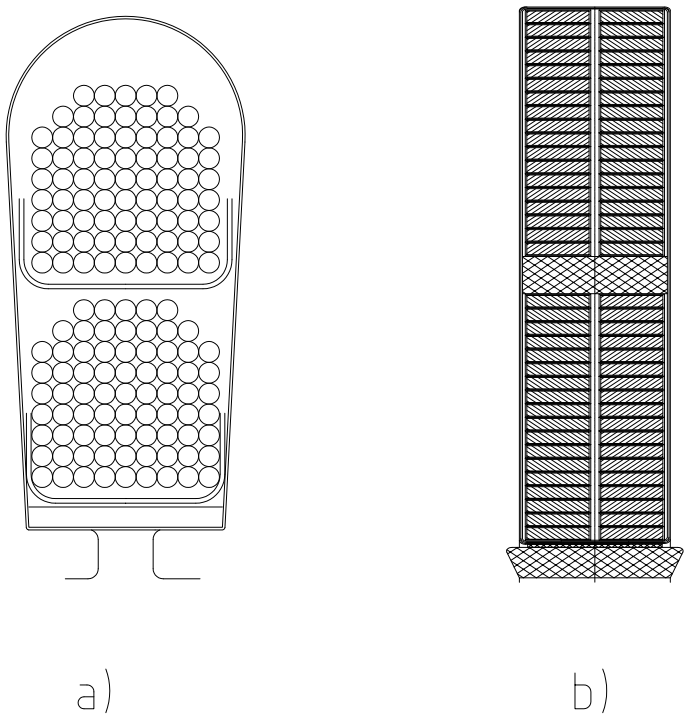

Figure 3-8: Different ways of arranging wire used in the turns of the coils: a) random wound (circular wire) b) form wound (rectangular straps)

, where θ_{ph} is the spatial angle measured with respect to the rotor magnetic axis, as shown in Fig. 3-9. The peak amplitude of this MMF is:

$$(\mathcal{F}_{ph})_{peak} = \frac{4}{\pi} \frac{k_w N_{ph}}{2p} \cdot I_{ph} \tag{3.14}$$

The single phase mmf wave is shown in Fig. 3-9:

The fundamental air-gap three-phase mmf wave of a distributed multi-pole winding can be easily obtained as:

$$\mathcal{F}(\theta_a, t) = \frac{3}{2}(\mathcal{F}_{ph})_{peak} \cdot \cos(p\theta_a - \omega_e t) \tag{3.15}$$

The three-phase mmf wave is shown in Fig. 3-10.

Under the assumption of a small air gap, the field winding can be assumed to produce sinusoidal radial space-fundamental air gap flux. Being g the air gap lenght,

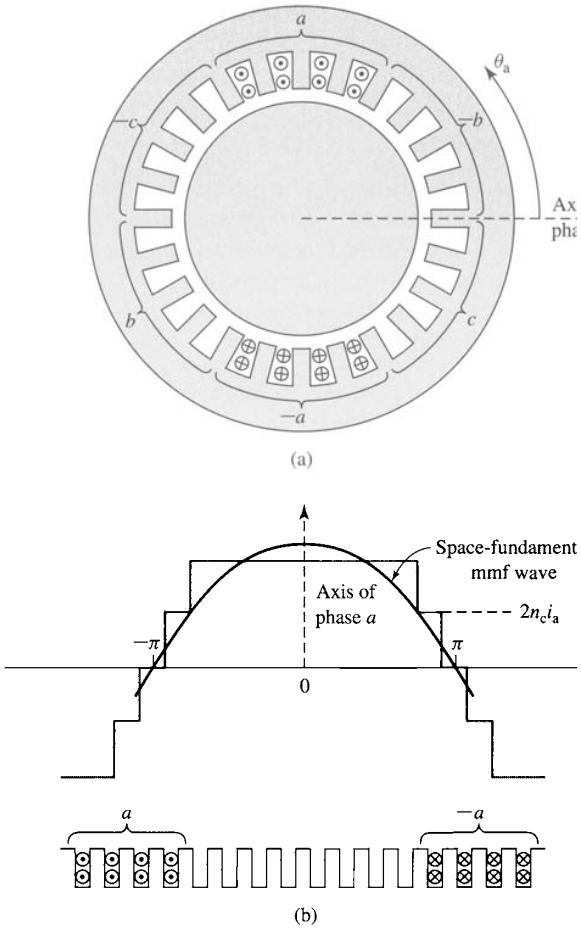

Figure 3-9: MMF of one phase of a distributed two-pole three-phase winding with full-pitch coils

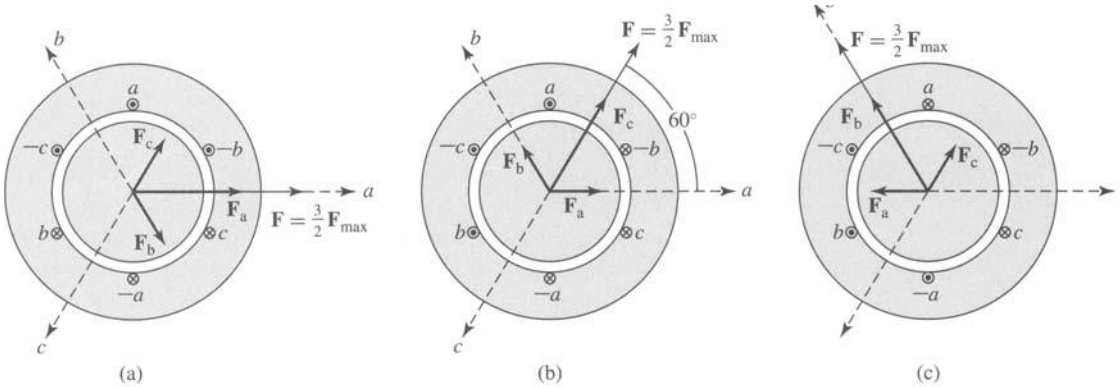

Figure 3-10: The production of a rotating magnetic field by means of three-phase currents on a simplified three-phase, two pole winding

the peak value of the flux density B [T] of one phase of the winding has the value:

$$B_{peak} = H_{peak} \cdot \mu_0 = \frac{(\mathcal{F}_{ph})_{peak}}{g} \cdot \mu_0 = \frac{4\mu_0}{\pi g}\left(\frac{k_w N_{ph}}{2p}\right) \cdot I_{ph} \tag{3.16}$$

The magnetic flux per pole Φ_p [Wb] is defined as the integral of the flux density over the pole area.

$$\Phi_p = l \int_{\frac{-\pi}{2p}}^{\frac{\pi}{2p}} Br \; d\theta_r \tag{3.17}$$

, where l is the axial lenght of the stator iron and r is the air gap radius. The flux linkage λ_{ph} is defined as:

$$\lambda_{ph} = k_w N_{ph} \Phi_p \cos(\omega_{me}) \tag{3.18}$$

being ω_{me} the electrical speed [rad/s] of the rotor. Finally, the induced electro-motive force, e, abbreviated emf, by Faraday's law, the voltage induced in any phase is

$$e_{ph} = -\omega_{me} k_w N_{ph} \Phi_p \sin(\omega_{me} t) \tag{3.19}$$

The maximum value of this emf is

$$E_{max} = \omega_{me} k_w N_{ph} \Phi_p \tag{3.20}$$

and the rms value is

$$E_{rms} = \sqrt{2} \; \pi f_{me} k_w N_{ph} \Phi_p \; = 4.44 \; f_{me} k_w N_{ph} \Phi_p \tag{3.21}$$

Chapter 4

Copper Losses and AC resistance

The evaluation of additional copper losses in synchronous or asynchronous machines within design and operation has been traditionally a difficult task with tedious equations that obscure the calculations, and this has lead engineers often to estimate or approximate them instead of calculating them. However, in the recent years with high probability in the near future, the increase in the utilization of the synchronous machines fed by inverters make the task of calculating the additional losses a necessary duty from the first stages of the electromagnetic and thermal design. Fig. 4-1 shows the typical composition of the losses in a PMSM.

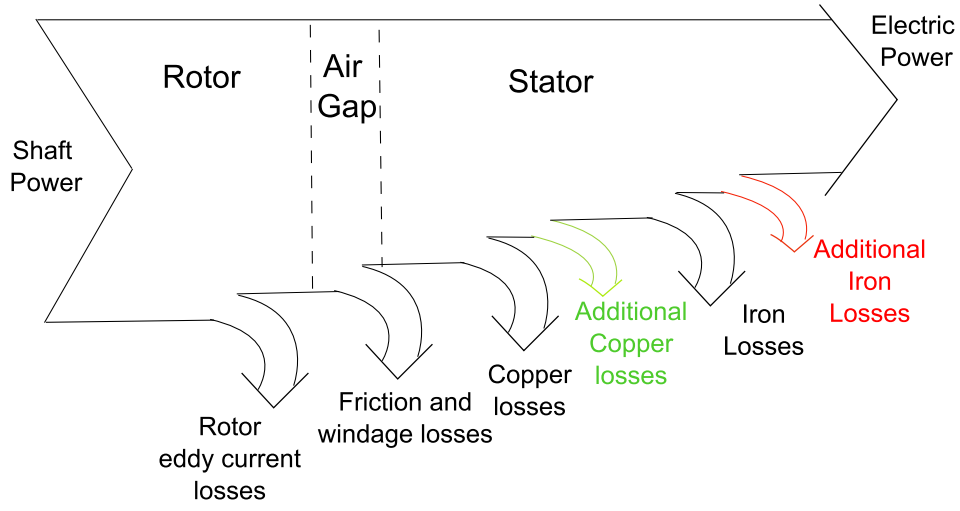

Figure 4-1: Composition of the losses in a Permanent Magnet Synchronous Generator

Additional copper losses usually represent about a 30% of the total losses of a PMSM, as depicted in Fig. 4-2 for the particular case of the G10x generator (note that the total additional copper losses would be constituted by the addition of the losses caused by the increment of the resistance at nominal frequency *i.e. red sector* and at the rest of frequencies *i.e. orange sector*):

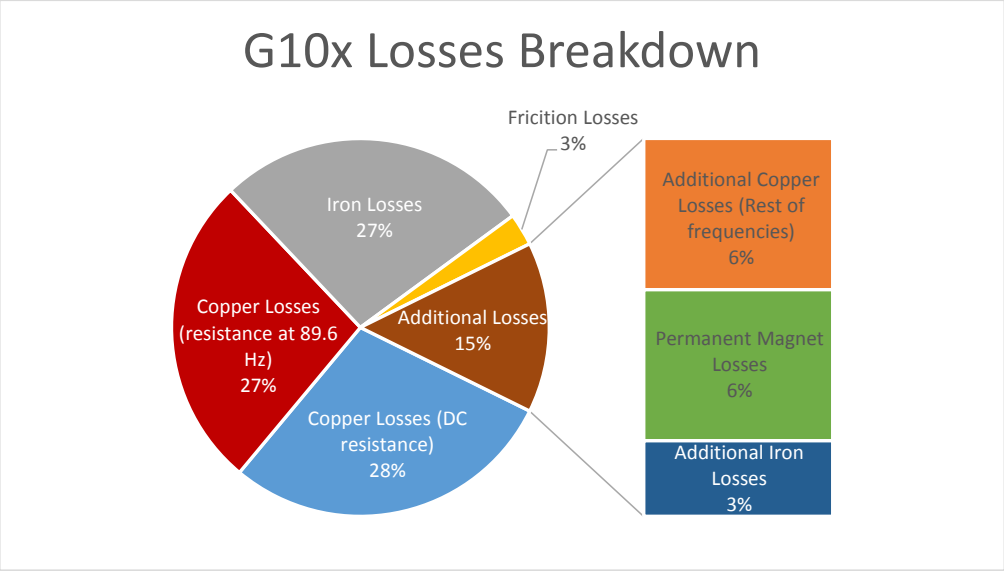

Figure 4-2: Loss Breakdown in the IPMSM G10x Generator. Font: Gamesa Electric

4.1 Skin and Proximity Effects

The particular phenomena that will be studied here in order to determine the *additional copper losses* in stator windings are the Proximity Effect Losses and the Skin Effect Losses in AC Windings, both related to the circulating Eddy Currents in the slot copper conductors. With the skin effect, described as the tendency of the current to flow on the outside of a conductor at higher frequencies, the current distribution is affected by the conductor's own magnetic field, increasing the losses. Proximity effect is similar, but is the mutual influence of multiple current carrying conductors. Their interaction causes uneven current distribution in the conductors, again increasing losses. Fig. 4-3 illustrates how the current distributes in a round wire when subjected to these effects.

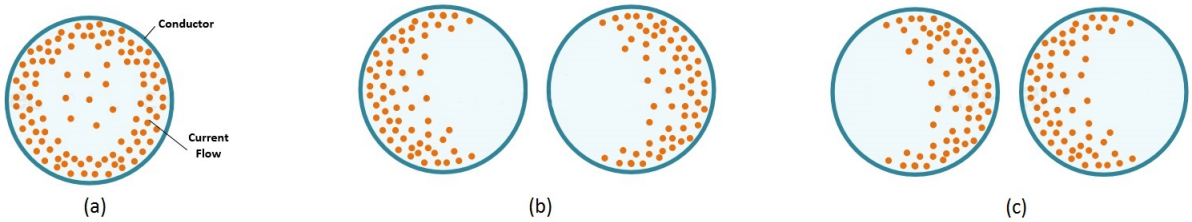

Figure 4-3: Current distributions over round wire for Skin effect (a) and Proximity effect: currents flowing in same direction, (b) and in opposite direction (c).

Proximity and skin effects are major source of losses in winding designs, as well as transformers, inductors, and AC power distribution systems composed of separate, round wire conductors, applied within enclosed pipe conduit. Whether the effect is visualized as induced circulating (eddy) currents, or as a redistribution of the current to meet boundary conditions, the result is a non-uniform current distribution with an increase in loss over what the DC resistance alone would suggest [9] [17].

Proximity effect can be considered as more dangerous than than skin effect. Besides, the analysis of proximity current losses is obscure and mathematically difficult (because of this, proximity effect is one of the most neglected magnetic design areas). It can be argued that core loss and proximity effect are the two most important considerations in magnetic design for AC stator windings, apart from the thermal considerations. Just as operating flux density is limited by iron additional losses (and not saturation) at high frequencies, so wire current density is limited by proximity effects, and not DC resistance.

4.2 Form Wound Stator Bars

If a form wound stator bar carrying an alternating current I_{bar} is considered [14], the skin effect will cause a current displacement towards the "'upper"' part of the bar: the slot bar forms a massive short circuit loop for the circulating eddy currents I_{Ft}, caused by the slot flux density B_Q that induces a voltage $u = -D\Phi/dt$ in the bar. The self flux of that eddy current, B_{QFt}, has opposite direction to B_Q due to Lenz's rule, and hence the eddy current I_{Ft} flows in the upper bar region with the same

direction to bar current I_{bar}, and in the lower bar region with opposite direction to bar current, as shown in Fig. 4-4.

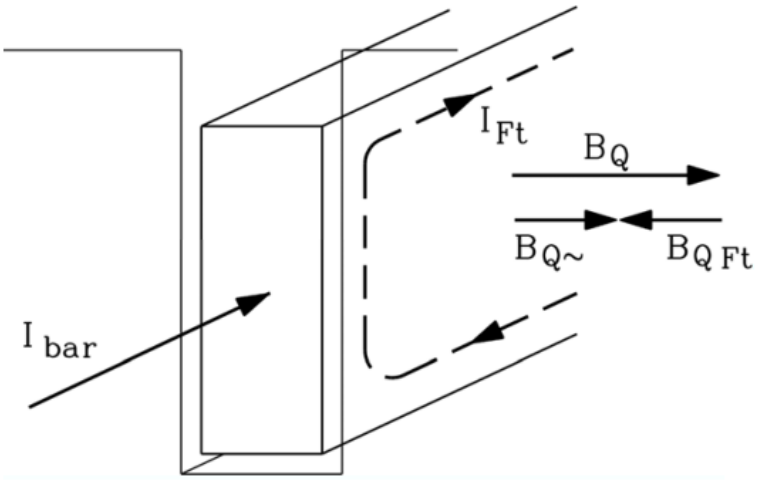

Figure 4-4: Circulating eddy currents in a form wound coil placed on a slot.

Due to those circulating eddy currents, the current density J_{bar}, defined as:

$$J_{bar} = \frac{I_{bar}}{A_{bar}} \tag{4.1}$$

presents an uneven distribution over the slot section, as one can realize in Fig. 4-5:

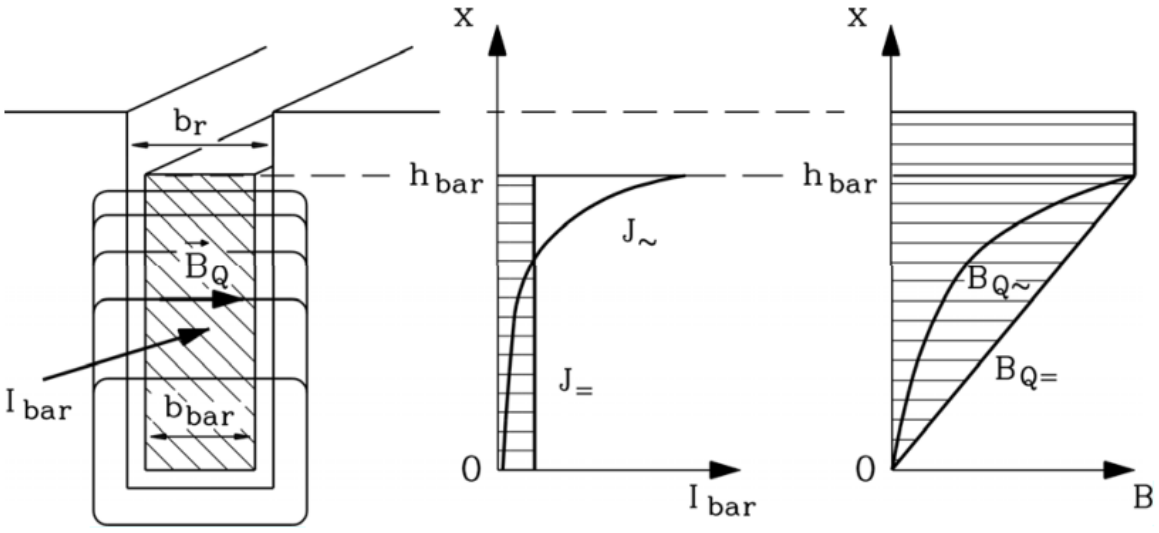

Figure 4-5: Current density displacement and flux density distribution in a form wound wire placed on a slot. $J_{\sim}$ and $B_{Q\sim}$ correspond to an alternate current and $J_{=}$ and $B_{Q=}$ to a DC current.

Therefore, the "AC bar resistance", $R_{bar\sim}$ is significantly higher than the "DC bar resistance", $R_{bar=}$. Similarly, due to a reduction in the stray flux density, the slot leakage flux is reduced. Hence the "AC bar inductance", $L_{bar\sim}$ is smaller than the "DC bar inductance", $L_{bar=}$ [18]. The relationship between the two resistances (DC and AC) and the two inductances (DC and AC) is called *relative increment*, and denoted by symbols k_R for the resistance increment and k_L for inductance increment:

$$k_R = \frac{R_{bar\sim}}{R_{bar=}} \tag{4.2}$$

$$k_L = \frac{L_{bar\sim}}{L_{bar=}} \tag{4.3}$$

The parameter *reduced conductor height*, ξ, is a per-unit value that contains the relevant information about the slot geometry:

$$\xi = h_{bar}\sqrt{\pi f \mu \kappa \frac{b_{bar}}{b_s}} \tag{4.4}$$

, being f the alternating frequency, μ the permeability of the conductor, κ the electric conductivity and b_{bar} and b_s the widths of the bar and slot, respectively. When this parameter is plotted against the relative increments of resistance and inductance, k_R and k_L, it is possible to observe the direct relationship between R/L increment and frequency:

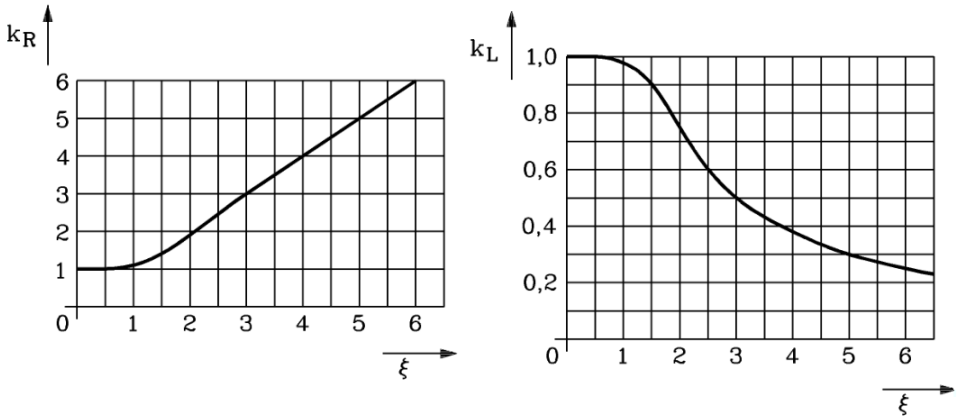

Figure 4-6: Resistance increase k_R and inductance decrease k_L with respect to ξ

Note that current displacement effect increases with increasing frequency f, with increasing electric-bar conductivity κ, with increasing conductor height h_{bar} and with increasing permeability μ of conductor. The next important parameter that needs to be considered is the *penetration depth*,d_E, that describes the decay of the current density inside a material (it is a measure of the depth at which the current density falls to 1/e):

$$d_E = \sqrt{\frac{b_Q}{b} \cdot \frac{1}{\pi f \mu \kappa}} \tag{4.5}$$

Now that all definitions and parameters are known, the equations describing the AC resistance increase for an stator winding may be derived.

4.2.1 Massive Form-Wound Bar Equations

The first case considered in order to clarify the calculations is the massive, solid copper bar placed inside the slot. The variables that need to be considered are described in Table 4.1.

Starting from Ampere's Law, the magnetic field in space around an electric current path can be described as:

$$\oint \vec{H} \cdot ds = \vec{J} \cdot \vec{A} = \kappa \vec{E} \cdot \vec{A} \tag{4.6}$$

Table 4.1: Initial variables for the derivation of AC resistance equations.

Symbol	Name	Units (SI)
Φ	Magnetic flux	[Wb]
H	Magnetic field strength	[A·m]
B	Magnetic flux density	[T]
E	Electric Field	[V]
I	Current intensity	[A]
J	Current density	[A/m^2]
b_Q	Slot width	[m]
b	Bar width	[m]
h	Bar height	[m]

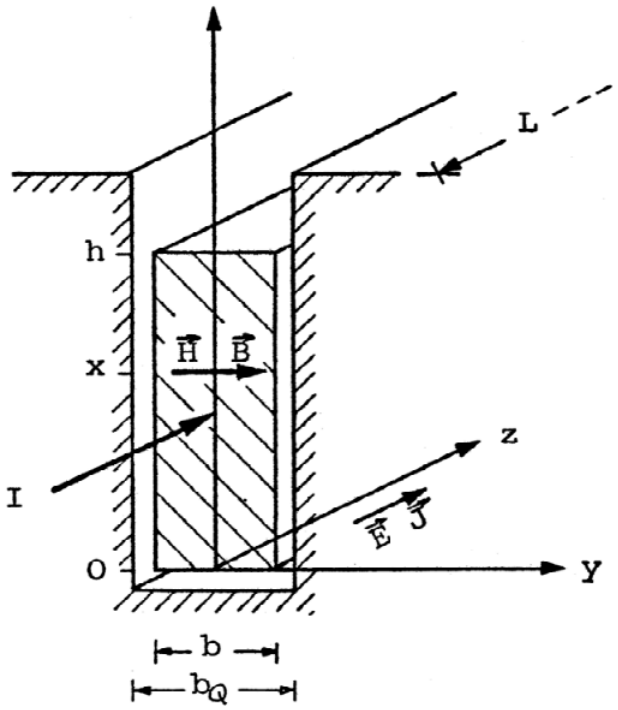

Figure 4-7: Massive slot conductor variables.

from which the first Maxwell equation for the electrical field in the slot direction, related to the magnetic field strength, is derived as:

$$\frac{\partial H_y}{\partial x} = \kappa \frac{b}{b_Q} E_z \tag{4.7}$$

and applying Faraday's law, that relates the electric field in a closed path with the magnetic flux:

$$\oint \vec{E} \cdot ds = -\frac{\partial \Phi}{\partial t} \tag{4.8}$$

one arrives to the second Maxwell equation:

$$\frac{\partial E_z}{\partial x} = \mu \frac{H_y}{t} \tag{4.9}$$

The solution of this partial differential equations for sinusoidal time functions yields the following result for the current density J_z:

$$J_z(x) = \frac{1}{\sqrt{2}} \cdot \frac{\omega \mu \kappa}{1/d_E} \cdot \frac{I}{b_Q} \cdot \sqrt{\frac{\cosh(2x/d_E) + \cos(2x/d_E)}{\cosh(2x/d_E) - \cos(2x/d_E)}} \tag{4.10}$$

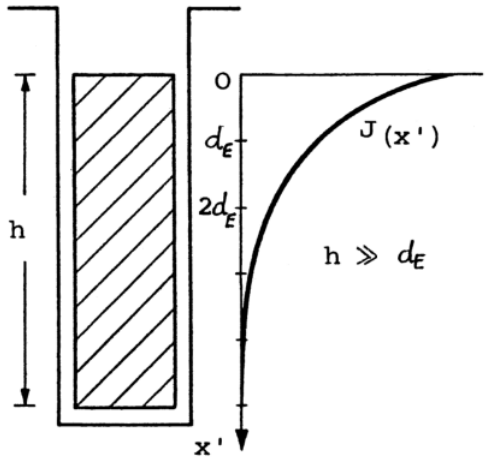

Figure 4-8: Current density $J_z(x)$ distribution on a massive conductor placed in the stator slot.

If the total losses in the conductor placed on a slot of width L are considered, then:

$$P_L = \frac{b \cdot L}{\kappa} \int_0^h J_z^2 \, dx = I^2 R_{\sim} = k_R \cdot I^2 R_{=} \tag{4.11}$$

and substituting J_z by the solution obtained in Eq. 4.10:

$$\begin{aligned} P_L &= \frac{b \cdot L}{\kappa} \int_0^h \frac{1}{2} \left(\frac{\omega \mu \kappa}{1/d_E} \right)^2 \left(\frac{I}{b_Q} \right)^2 \cdot \frac{\cosh(2x/d_E) + \cos(2x/d_E)}{\cosh(2x/d_E) - \cos(2x/d_E)} \, dx = \\ &= I^2 \cdot R_{=} \cdot \xi \cdot \frac{\sinh(2x) + \sin(2x)}{\cosh(2x) - \cos(2x)} \end{aligned} \tag{4.12}$$

Therefore, the coefficient k_R for the relative losses increment is:

$$\boxed{k_R = \frac{R_{\sim}}{R_{=}} = \varphi(\xi) = \xi \cdot \frac{\sinh(2\xi) + \sin(2\xi)}{\cosh(2\xi) - \cos(2\xi)}} \tag{4.13}$$

which in this case, as only one massive conductor slot is considered, is only related to skin effect and not to proximity effect.

However, if only one massive conductor slot was used in the stator windings, the additional losses would be huge, as shown in the comparative Table 4.2, so the first consideration is to reduce the conductor height by means of adding a certain number of series turns in the coil, so that h is reduced.

Table 4.2: Comparative on losses depending on conductor height, Cu bar at 50 Hz, $\kappa = 5e^7$ 1/m, $\mu = \mu_0$, b=b_Q,d_E=0.01m

Conductor Height h [m]	k_R [-]
0.005	1.0
0.01	1.09
0.04	4.0
0.1	15.6

4.2.2 Split-Conductors Form-Wound Bar Equations

As evinced in the previous section, the placement of a massive conductor along the slot length is not viable due to the huge increase of AC resistance as the critical conductor height is surpassed. Hence, this height must be reduced in order to decrease skin effect losses. The way to to this is to wind the coil in several series turns, so that now each turn behaves like a massive conductor, and the conductor height h is now the individual conductor height (see Fig. 4-9). However, as several conductors

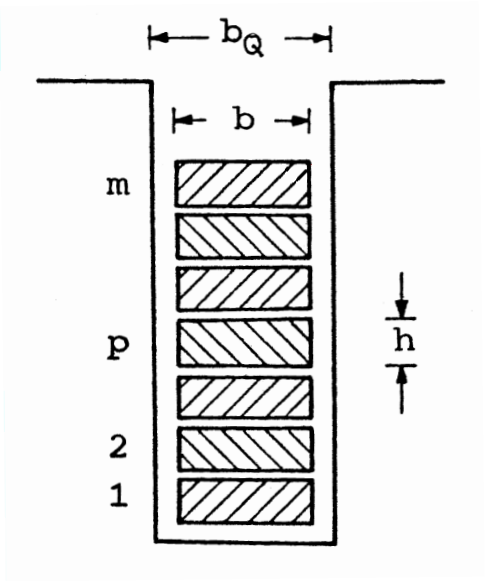

Figure 4-9: Division of the conductor in series strands: m is the number of series conductors and h is now the individual conductor height.

are now placed one next to another, they will suffer from proximity effects; the lower conductor experiences only its own slot stray flux, i.e.

$$k_{R,1} = \varphi(\xi) \tag{4.14}$$

, but the next conductor will experience its own stray flux plus the proximity flux coming from the turn below:

$$k_{R,2} = \varphi(\xi) + 2\psi\xi \tag{4.15}$$

and for the p^{th} turn:

$$k_{R,p} = \varphi(\xi) + p(p-1) \cdot \psi(\xi) \tag{4.16}$$

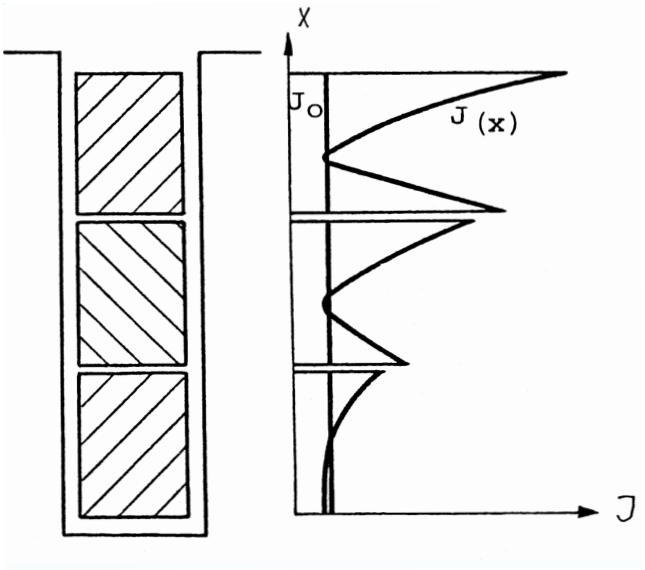

Figure 4-10: Current density $J_z(x)$ distribution on a split conductor (several number of series turns) placed in the stator slot.

The value of $\psi(\xi)$ can be expressed as:

$$\psi(\xi) = 2\xi \cdot \frac{\sinh(\xi) - \sin(\xi)}{\cosh(\xi) + \cos(\xi)} \tag{4.17}$$

The average increase of the AC resistance across the slot with m series conductors is:

$$\boxed{k_{R,m} = \varphi(\xi) + \frac{m^2 - 1}{3}\psi(\xi)} \tag{4.18}$$

4.3 Final formulations

Some considerations must be done when rest of the parameters of the geometry is considered, in order to get an accurate result in the calculation of the additional losses. These are:

- The number of layers in the windings.
- The disposition of parallel conductors inside one branch.
- The consideration of the end-winding geometry.
- The use of some manufacturing techniques in order to reduce additional losses.

4.3.1 Double Layer Windings

If a double-layer winding geometry is used, as the one shown in **??** (b), the value of the number of turns per coil, m, is doubled. Besides, the mutual induction or proximity effect between the two layers must be corrected by means of the introduction of the correction factor k_y in Eq. 4.18:

$$k_{R,m} = \varphi(\xi) + \frac{m^2 - 1}{3}\psi(\xi) \cdot k_y \tag{4.19}$$

This correction factor depends in the value of the shortened pitch; for a three-phase arrangement of the winding, its value is taken as the one depicted in Fig. 4-11. On the other hand, the number of conductors in the circumferential direction does not produce extra losses: the only parameter that is affected is the relationship between b and b_Q, because of the copper-free space, so the difference in the final result is not significant.

4.3.2 Parallel winding branches and conductors

When the coil is manufactured using several parallel conductors, the conductor height h is now the height of the parallel conductors that together form one turn of the coil;

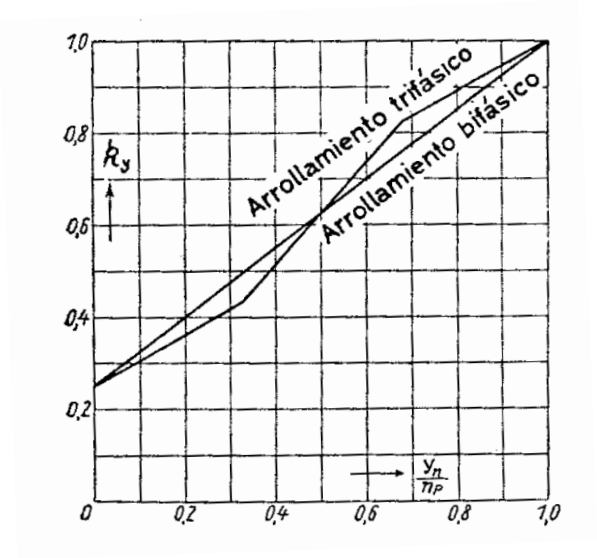

Figure 4-11: Correction factor k_y for the calculation of additional losses in shortened-pitch double layer windings.

on the other hand, the number of turns per coil m, is the number of series-connected set of parallel conductors that form all the turns of the coil (see Fig. 4-12).

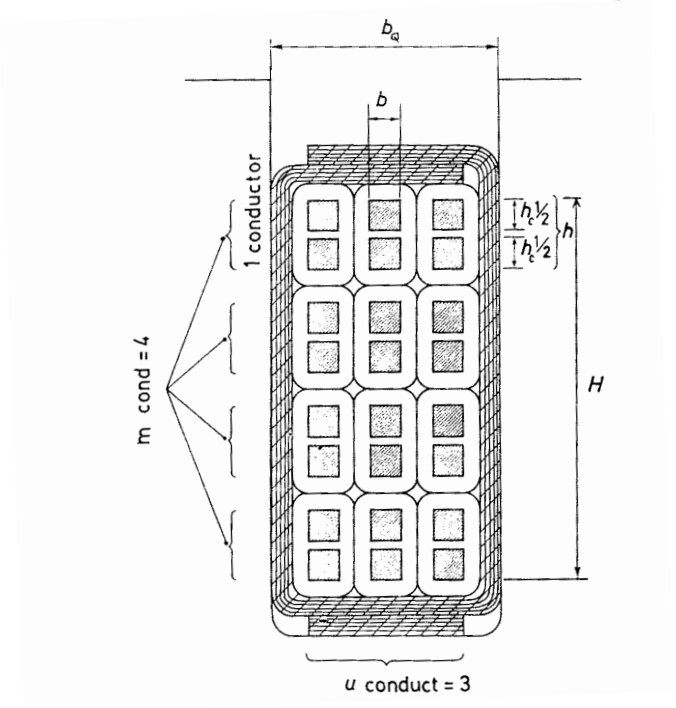

Figure 4-12: Characteristic dimensions of a double-layer winding arrangement with six parallel conductors per turn (2 parallel conductors in height).

4.3.3 End winding geometry

The end winding geometry affects the calculation of additional losses , as the skin and proximity effects are greatly reduced at the winding overhangs. Therefore, the average factor for the slot and the end winding, that is, the entire geometry of the winding, must be calculated as:

$$k_{Rtot} = 1 + (k_R - 1)\frac{2L_{fe}}{L_{av}} \tag{4.20}$$

, where L_{fe} is the equivalent length of the iron core, and L_{av} is the average length of the coil turn.

4.3.4 Additional Losses minimization methods

The skin and proximity effects can be minimized with the following methods:

- The most effective method is to divide the conductors into subconductors, as shown in Section 4.2.2. As this conductors are transposed due to end-winding overhang, the stray flux is reduced. If each of the strands of one coil is soldered individually in series with the corresponding strand of the next coil, without paralleling the strands, a complete elimination of slot stray flux is possible. However, this is time-consuming, and requires expensive manufacturing.

- Instead of dividing the bulky conductors into subconductors, parallel paths can be used, that is parallel-connected poles and group of poles. If the number of parallel paths is a, the series-connected turns must be a-fold in order to keep the branch voltages (and thus the air-gap flux density) constant. This means that the conductor height is reduced in the ratio of $1/a$.

- Using twisted conductors with perfect conductor transposition, arranged using multi-thread strands, as the Roebel bar (see Fig. 4-13) or the Litz wire.

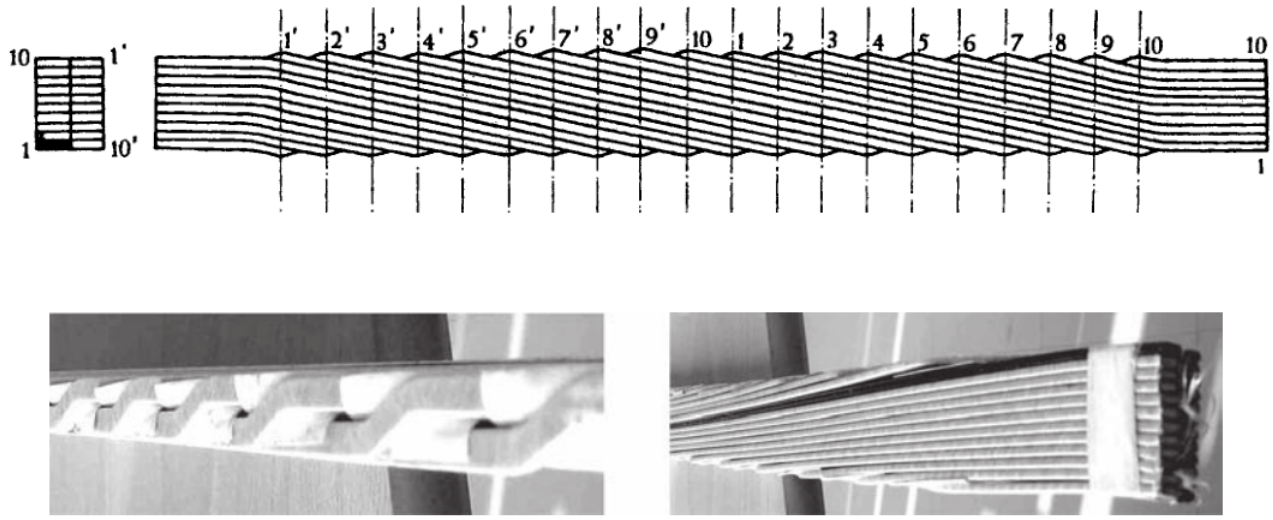

Figure 4-13: Roebel bar schematics and photographs. The Roebel bar has minimal skin effect in a slot because of its perfect transposition

Chapter 5

Computer Tool

5.1 Introduction to PROCAP tool

The ultimate purpose of this thesis is the realization of a computer tool to aid the first stages of the design of a IPMSM. The tool is thought to be time-saving, so the computation time must be one of the key factors taken into account. It is mandatory that the functionality of the tool is maximized not only for additional losses, but to give a general overview about the electric behavior of the machine in steady state. It has also been taken into account that the users of this tool may not be familiar with the electric transient simulation program (Matlab Simulink) used. Therefore, an intuitive interface must be created in order to make this tool available for all electric / electronic engineers, no matter their specific knowledge about the specific simulation software. This interface has been realized in Spanish as it is the local language of the company that it has been deigned for, and it has received the name "Programa para Calculo de Perdidas Adicionales", or PROCAP.

The basic structure of the program is the following: the relevant input parameters (modulation set up, geometry of the machine) are requested to the user, and they are introduced into the core of this program, the Simulink model of the modulation and the PMSM. Then, once this model is executed, the resulting data from voltages and currents is obtained, and a FFT analysis is performed in order to characterize the exact composition of the waveforms. The copper losses of the machine are calculated

and finally the results are plotted and shown in the interface. Fig. 5-1 shows the basic flowchart of the interface.

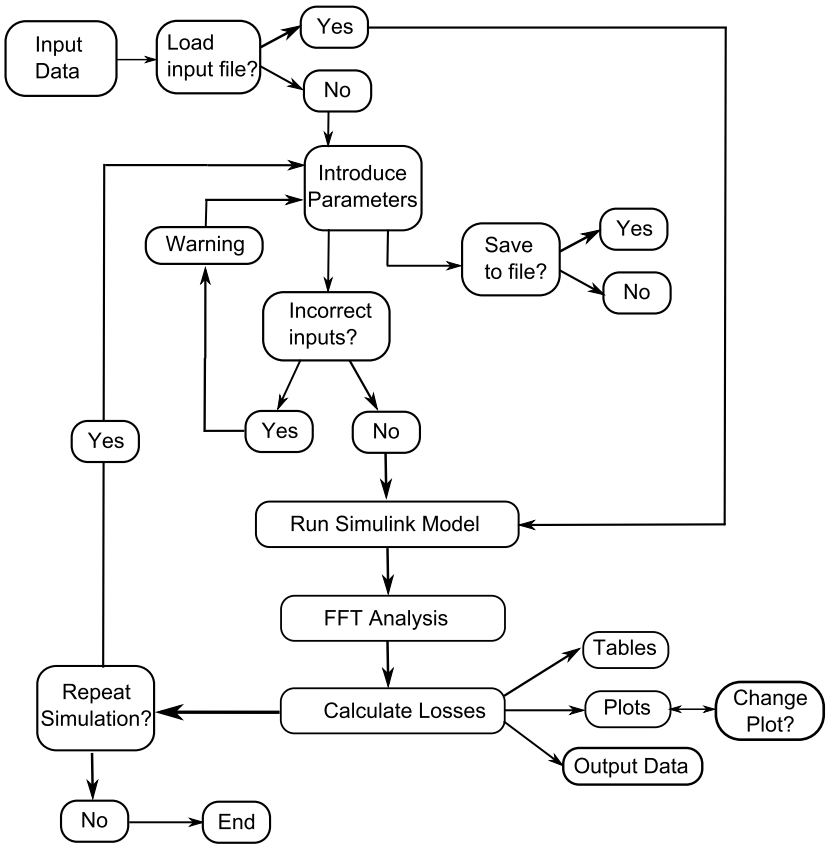

Figure 5-1: Basic flowchart of the PROCAP Graphical User Interface.

The additional features included in this program are:

- Save parameters to file/ Load parameters from file .
- Choose different types of modulation: SVPWM, SPWM, 3-level SPWM.
- Spectral Resolution Selection: from 0.1 Hz to 10 Hz.
- Quick Plot Selection and Navigation.
- Table of Harmonics, Impedances, Inductances and Power Losses.
- Save results to Excel format (.xls) file.

5.2 Simulink Model

The proposed Simulink model includes the modulation, the LCR filter and the machine. All the relevant parameters can be modified from the main interface of the graphical tool, and the simulation is launched also from there, so that the simulation runs in the background and the end user does not notice about it as long as the Simulink file is not explicitly opened. The general layout of the model is shown in Fig. 5-2.

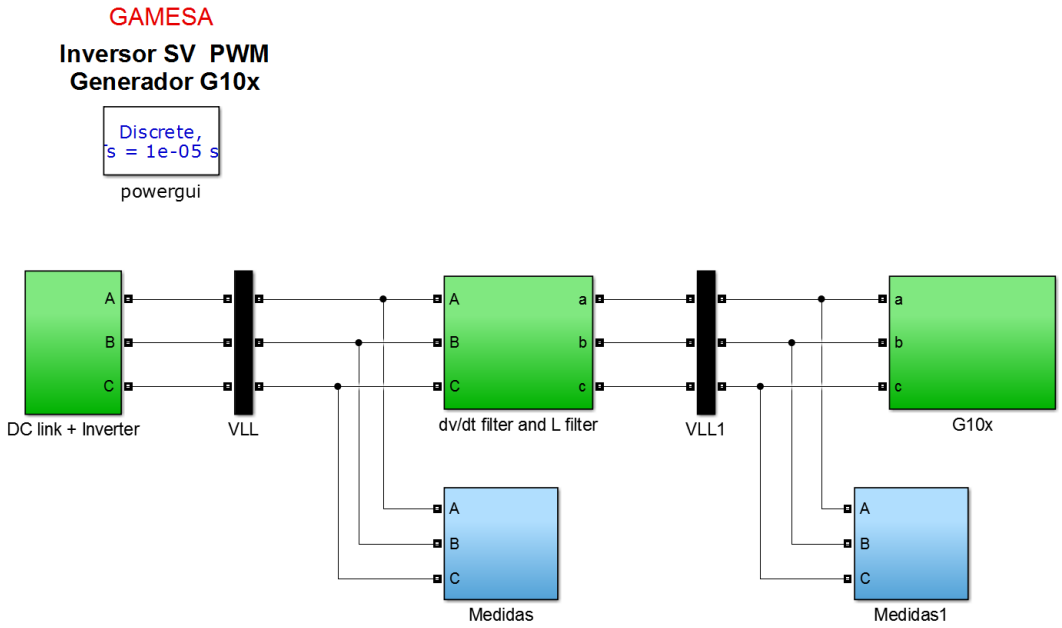

Figure 5-2: Simulink model of the Converter, Filter and IPMSM

The converter is modeled using the block "'Universal Bridge"' for the case of the two-level inverter, or the block "'Three-level Bridge"' for the case of the 3-level NPC inverter, both from Simulink Library. The control is made in open loop so that the modulator internally generates the reference signal using the modulation index and the output and carrier frequencies. Fig. 5-3 shows the inverter model, that allows to select between two or three level inverters, and SVPWM or SPWM modulations. The special case of the SV-PWM modulation has been developed specifically with the purpose of analyzing the set of voltage harmonics depending on the placement of the zero-vectors used, leading to different harmonic compositions. Fig. 5-4 shows the development process of the SV-PWM modulation.

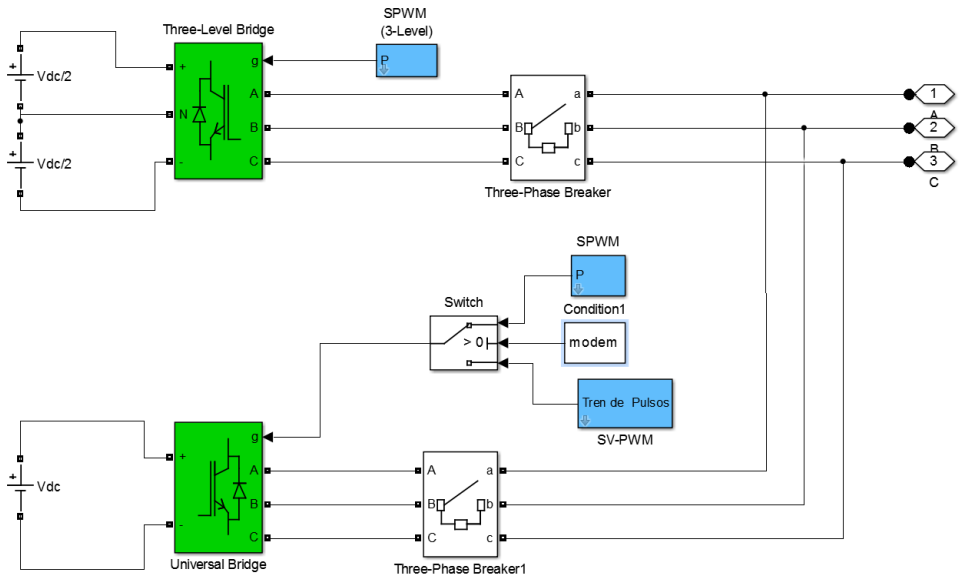

Figure 5-3: Simulink model of the inverter

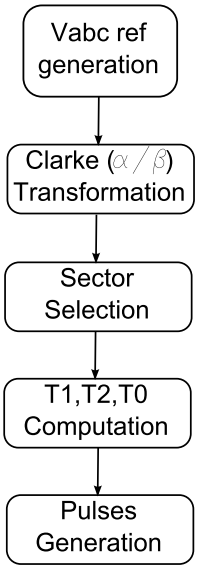

Figure 5-4: Schematic diagram of SV PWM modulation and inverter pulse generation

The filter used is a LCR filter in series between the converter and the generator, which will attenuate some of the high frequency components of the input voltage to the machine, as well as shorten the voltage peaks (acting as a dv/dt filter).

The machine has been modeled using the PMSM block from the Simulink library.

5.3 Graphical Layout

The initial graphical layout of the tool developed can be seen in Fig. 5-5. The initial view to the program shows that there is a space reserved for typing the input parameters, and another one dedicated to plotting the results. The task of typing all the input parameters might be considered tedious as they are not few; therefore the "Load Parameters" and "Save parameters" features have been added so that the user only has to type the parameters once, allowing to save a lot of time when iterative calculations wish to be performed.

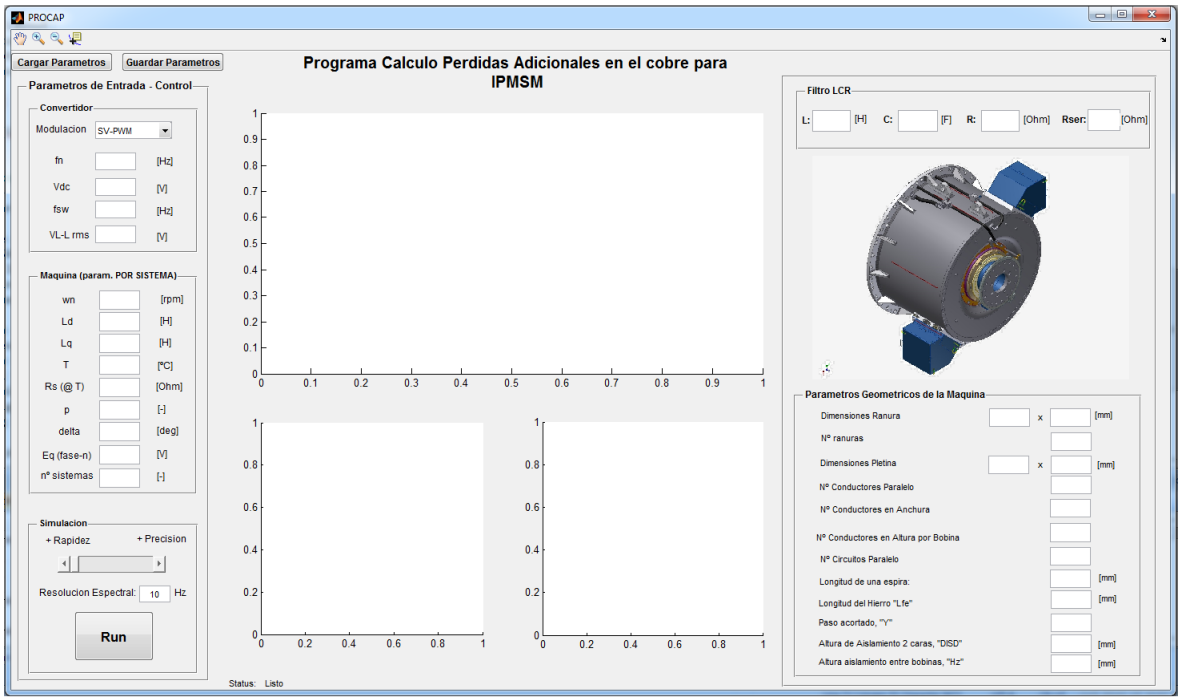

Figure 5-5: Input parameter stage screen of the graphical analysis tool.

The upper-left side part of the program is dedicated to specify the converter, or control parameters, in which it is possible to select among the three different types of modulation (SPWM, SVPWM and three-level SPWM), as well as the input parameters to the inverter: DC bus voltage, switching and natural output frequency, and line-to-line output voltage amplitude. Immediately under that section, there is a space reserved for the electrical parameters of the machine: L_d, L_q, R_s, nominal speed, delta angle, number of pole pairs, nominal back-emf, etc, while the geometrical

parameters of the machine, the ones that define the winding geometry, are requested in the right part of the program. The LCR filter values can be changed in the upper-right part of the program.

The main simulation setting feature that has been added can be observed in the lower-left part of the program; here the spectral resolution can be changed in order to get more *frequency domain resolution* (well-defined fft peaks), which will cause the total simulation time to be significantly higher; or less spectral resolution, which will lead to lower quality on the FFT performance but will allow a faster simulation capability. Even though the lower quality of the FFT will lead to inaccuracy in the losses calculation, the results for all the spectral resolution allowed are acceptable, with a range of variation of less of 2% of the total losses. This resolution selection can be very useful in the industrial domain, when sometimes the company offers a product and does not want to lose time in calculations; in this case the accuracy is not very important. On the other hand, once the design process has started, the accuracy gains relevance and the simulation times are accepted to be longer. However, the maximum simulation time that has been registered (setting the spectral resolution to the finest level) has been lower than 1 minute, so in any case the program will burden the design process with an excessive calculation time.

Once all the input parameters are set, the push-button "Run" can be pressed, and the simulation starts. If there is any incorrect number or a blank space in one of the parameter boxes, the program will show with a warning dialog indicating the mistake, and those parameters will be set to a default value, corresponding to the G10x generator parameters.

5.4 FFT Analysis

One of the cores of this program is the Fast Fourier Transform (FFT) analysis, which is internally performed once the Simulink model is executed, simulated, and finished, and all the data from voltages and currents is stored. The FFT process implies selecting an adequate number of samples, far enough from the starting point, but large

enough in order to give the desired spectral frequency. Being N the total number of samples taken for the frequency analysis of the input voltage/current waveform, and $T_s = 1/f_s$ the sampling period in the time domain, the total analyzed time is:

$$t_{total} = N \cdot T_s \tag{5.1}$$

And the inverse of this number will be the spectral resolution that the FFT will have, in Hertz:

$$f_{res} = \frac{1}{N \cdot T_s} \tag{5.2}$$

If a clean, perfectly defined FFT plot is desired, one should notice which is the Minimum Common Divisor (MCD) of all the frequencies that will take part of it; as an example, if the target output natural frequency of the voltage is 89.6 Hz, and the switching frequency 5000 Hz, and bearing in mind that the harmonic side-bands appear at:

$$\begin{aligned} f_s &\pm k \cdot f_n \\ 2 \cdot f_s &\pm 2k \cdot f_n \\ 3 \cdot f_s &\pm k \cdot f_n \end{aligned}$$

and successive multiples of them, $\forall k \in \mathbb{Z}$, then the adequate spectral resolution required would be in this case 0.8 Hz, as it is the MCD of all that numbers. If, for example, a 10 Hz resolution is selected, the output FFT peaks will appear to be built from several grouped bands, called *dispersionbands*, around the multiple frequencies that compound the wave. Fig 5-6 shows the difference between these two cases, which is the same difference explained in the previous section, when the *accurate* and $fast$ configurations of the program were explained. However, the inaccurate result can also be somewhat useful; the resulting amplitude may be obtained by applying the concept of dispersion energy: The virtual current amplitude i_v of the harmonic h,

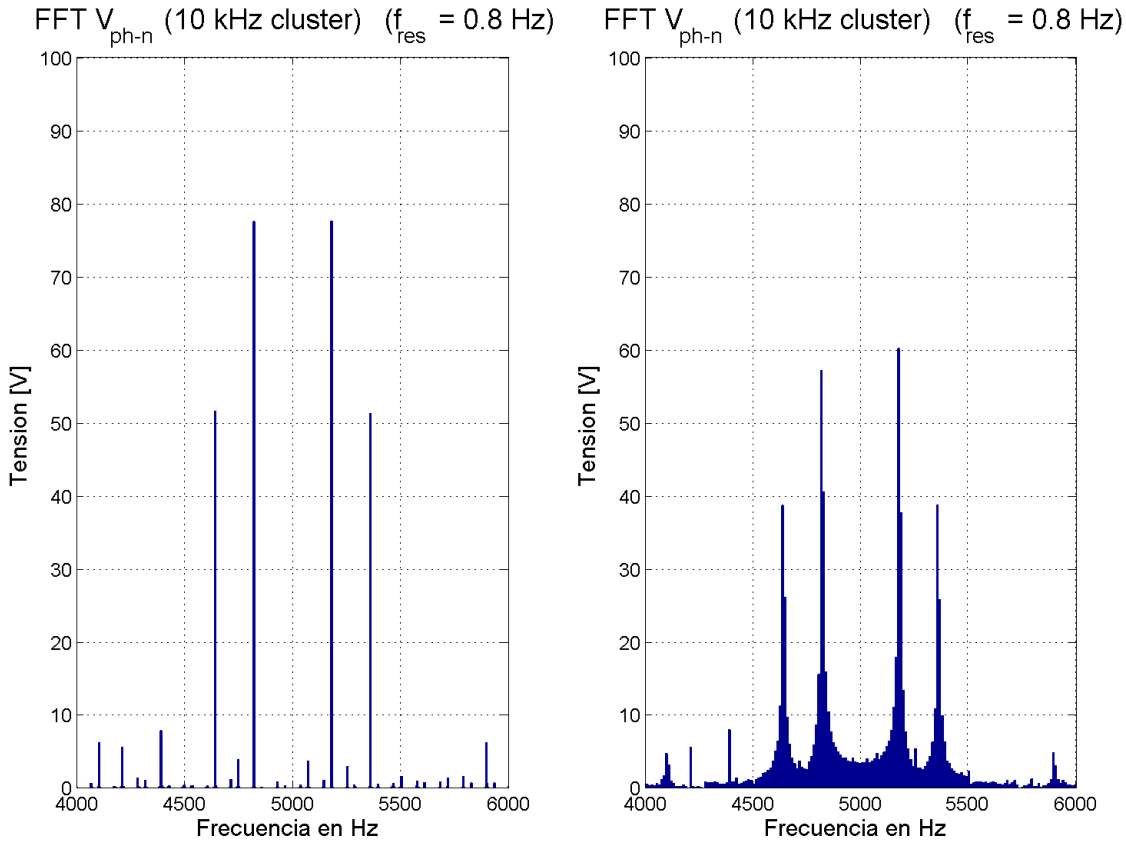

Figure 5-6: Two different FFT analysis of the same voltage waveform: 0.2 Hz resolution (left) and 10 Hz resolution (right)

located in the center of the dispersion band, which has an spectral energy:

$$E = i_v(h)^2 \tag{5.3}$$

can be estimated from the "'n"' dispersion components around it, as their energy will be the same:

$$E = \sqrt{i(h-n)^2 + ... + i(h-1)^2 + i(h)^2 + i(h+1)^2 + ... + i(h+n)^2} \tag{5.4}$$

so that if n is chosen carefully to comprise all the dispersion band, but not to affect to other lateral bands, the resulting current amplitude and thus the losses can be estimated with a very low error.

Moreover, in order to reduce the amount of data managed once the FFT is performed, only the points containing relevant information are plotted; the rest of points, in which the amplitude of the current or voltage is zero or nearly zero, are dismissed.

When the dq transformation of the currents and voltages is obtained and the FFT is performed to that waveform, one can realize that the stator currents and voltages are effectively turning in both directions around the stator windings: Fig. 5-7 shows the FFT analysis of v_{dq}.

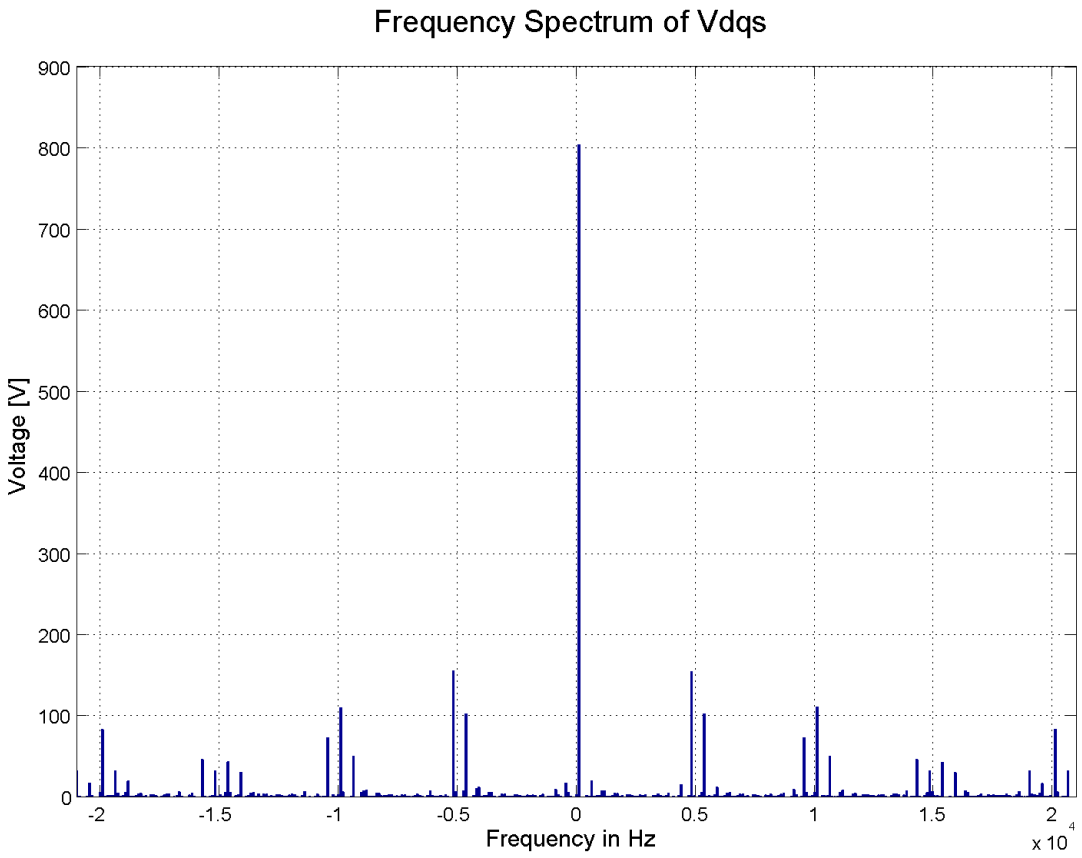

Figure 5-7: FFT analysis of v_{dq} in 2-level SV-PWM modulation.

5.5 Evaluation of losses

Once the current FFT is well defined, the losses are calculated as indicated in Chapter 4. Each of the components of the current spectral decomposition is introduced in

formula 4.20, and the resulting Cu losses for the DC and AC resistances are broke down before adding them together to give a total amount of copper losses of the machine, as shown in Fig. 5-8 One can observe that the percentage of losses presented

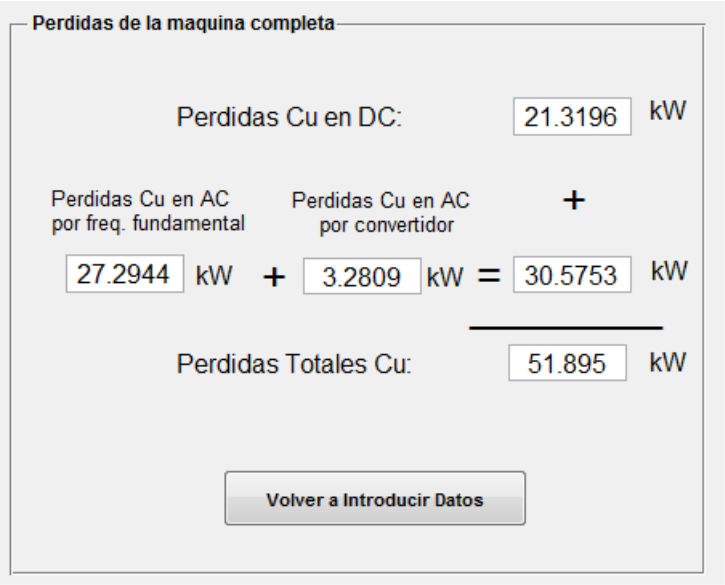

Figure 5-8: Losses Breakdown shown in the Computer Tool's results palette

in Fig. 4-2, is effectively accomplished. The stator DC resistance will cause a certain amount of DC copper losses, which are expected to be doubled (depending on the design, this number may usually vary from 75% to 125% of the DC Cu losses) at the natural output frequency (89.6 Hz in this case). The rest of the frequencies, representing the losses induced by the converter, represent a lower percentage of the total losses (less than 25% of the DC Cu losses, and therefore less than 10% of the total Cu losses of the stator).

5.6 Program Outputs

As already commented, this computer tool provides the user with the most important relevant information about the input (simulated) waveforms, as well as the copper losses of the machine, and allows the user to manage the information by means of the introduction of useful tools in the Graphical Interface of the program. The first useful tool consists on the graphical representation (plots) of the selected waveform/FFT

analysis. One of the nice things about this feature is that, once simulated, the user can navigate through the plots without the need of running the Simulink model and performing the FFT again, so it makes it instantaneous to change from one to another. The different output waveforms that can be plotted are:

- Stator Voltages (phase to neutral and phase to phase) and Currents.
- FFT of the voltages.
- FFT of the currents.
- FFT of the dq transform of voltages and currents.

Fig. 5-9 shows how the final screen would look like if the user plots the Stator Voltages and Currents (plotted by default once the simulation and analysis is finished). Fig. 5-

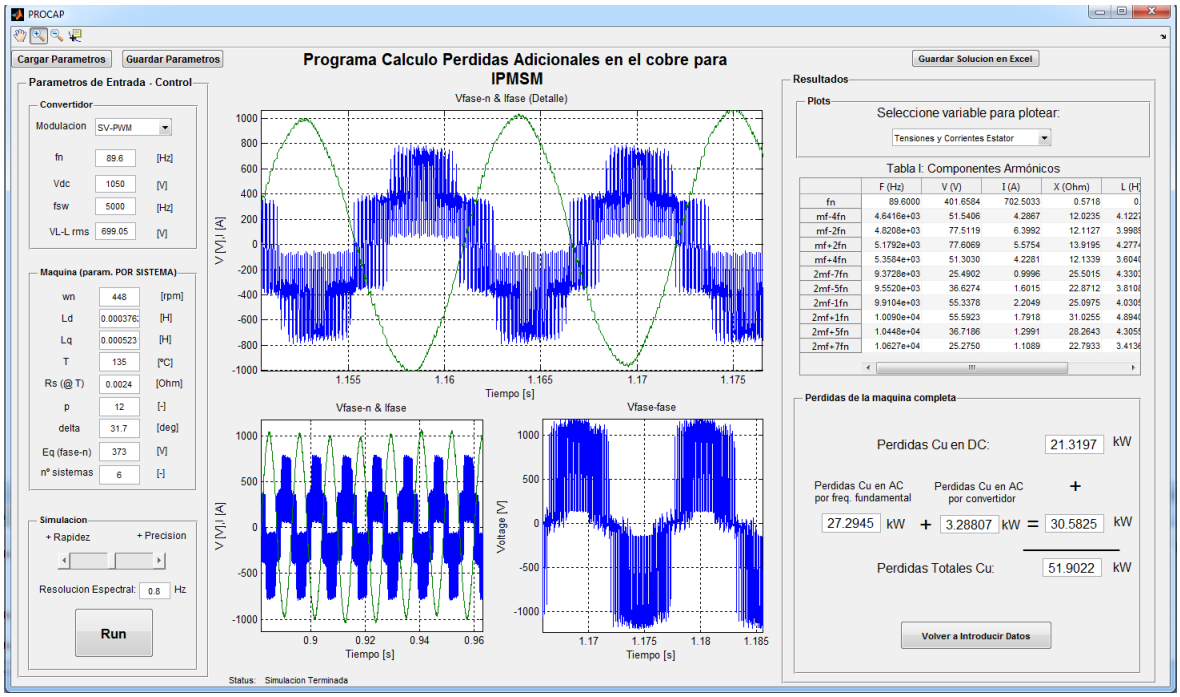

Figure 5-9: Aspect of the Graphical Tool once the simulation and analysis is performed. Stator Voltages and Currents plot selected.

10 shows how the output screen looks like if the FFT of the stator phase-to-neutral voltage is plotted. Note that the two most important clusters, produced at f_{sw} and $2f_{sw}$ are emphasized in the lower plots, while the whole harmonic spectra is shown in the upper plot.

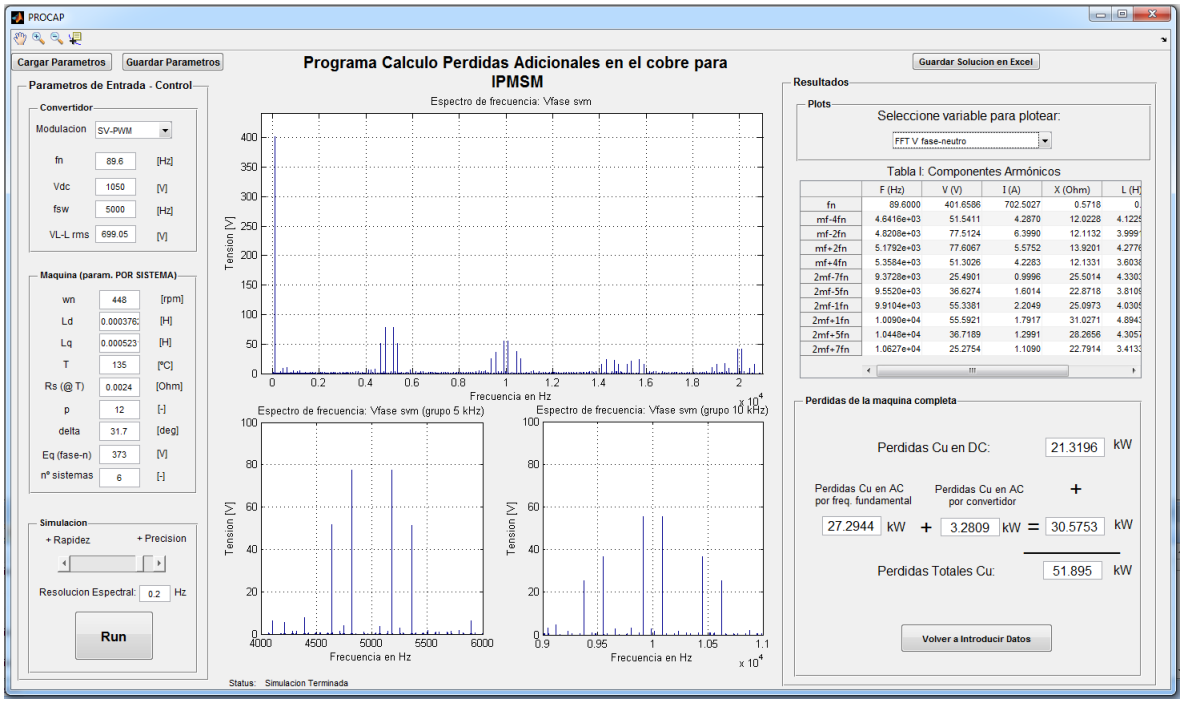

Figure 5-10: Aspect of the Graphical Tool once the simulation and analysis is performed. FFT of the stator phase-to-neutral voltage is plotted.

If the three-level NPC inverter modulated with the standard sinusoidal PWM technique is selected, the output voltage and current waveforms will change, the switching is made using a different technique and thus their harmonic composition is also modified. The characteristic line-to-line voltage waveform can be seen in 5-11 (a). The phase-to-neutral voltage and the phase current are shown in Fig. 5-11 (b).

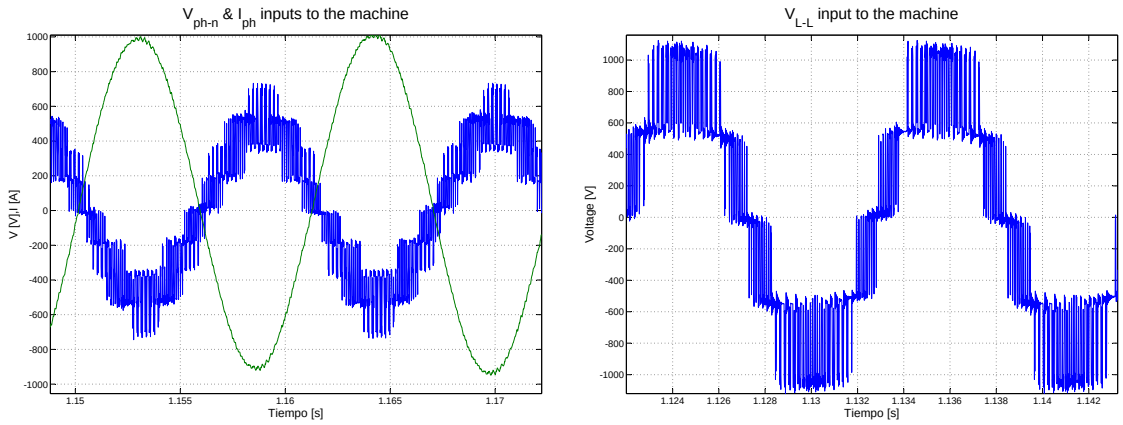

Figure 5-11: Phase-to-neutral voltage and current (left) and line-to-line voltage waveform (right) of the 3-level inverter with sinusoidal PWM modulation.

The harmonic composition of the 3-level line-to-neutral voltage is depicted in Fig. 5-12, which compared to the 2-level SV-PWM is quite different in the side-bands around the switching frequency. The THD in 3-level SPWM is significantly lower

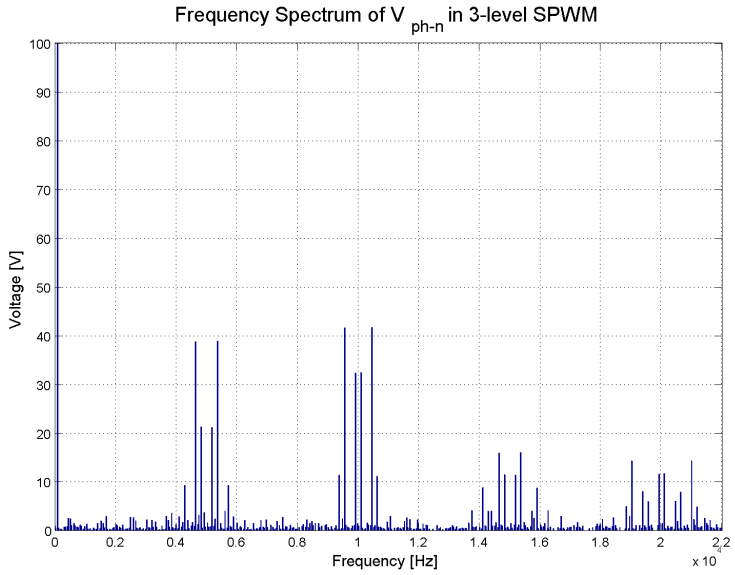

Figure 5-12: Frequency Spectrum of V_{ph-n} in 3-level S-PWM

than in the 2-level SV-PWM, and much lower than in the 2-level SPWM. However, here it is supposed than the switching frequency would be the same when comparing them, but in reality the 3-level switching frequencies are much lower (hundreds of Hz) than the 2-level switching frequencies (thousands of Hz), worsening the THD of the 3-level output, and thus leading both techniques to present a similar THD at the output voltage. Obviously, the advantage of using lower frequencies is the reduction of the switching losses.

Another important output feature of the program is the *table* shown in the right part of the solution screen, where the relevant harmonic frequencies are listed with their harmonic order, as well as their corresponding voltages and currents magnitudes, the impedance and inductance seen at those frequencies and the power loss that they represent (see Table 5.1 for the solution of the G10x machine as an example). The impedance is calculated by direct application of Ohm's law, $X = V/I$ and the

Table 5.1: Harmonic composition of the machine losses.

	F (Hz)	V (V)	I (A)	X (Ohm)	L (H)	P (W)
fn	98.6	368.6	682.6	0.54	9.5e-4	45909
fsw-4fn	4641.6	33.8	2.6	12.8	4.3e-4	129.6
fsw-2fn	4820.8	30.1	2.0	15.0	4.95e-4	76.4
fsw+2fn	5179.2	30.0	2.1	14.1	4.34e-4	87.7
fsw+4fn	5385.4	33.9	2.0	16.2	4.82e-4	86.0
2fsw-7fn	9372.8	20.9	0.8	25.4	4.32e-4	17.2
2fsw-5fn	9552.0	38.2	1.6	23.3	3.88e-4	69.11
2fsw-1fn	9910.4	28.3	1.12	25.1	4.03e-4	33.39
2fsw+1fn	10089.6	28.4	0.9	31.0	4.89e-4	22.25
2fsw+5fn	10448	38.3	1.3	28.1	4.28e-4	49.97
2fsw+7fn	10627	20.7	0.9	21.7	3.25e-4	24.7

inductance is found as that impedance value divided by the corresponding angular frequency.

Finally, the program allows to save the relevant output data (Voltages and Currents plots, and also their FFTs, losses breakdown, and the table commented in the previous paragraph) in different sheets of a new Excel (.xls) file by just clicking a button.

All the features shown make PROCAP program a useful, fast, user-friendly tool that covers some of the important design parameters of IPMSM, providing an exhaustive harmonic analysis of the input voltages and currents, an accurate breakdown the copper losses, and the possibility to export or save the results, as well as the input parameters.

The results of the A-type machine that have been tested have been compared to real experimental data taken in the factory's test bench.

5.7 Model Validation

The A-type machine experimental data taken in the test bench is correlated with the results of the simulation. The converter setup is made using SV-PWM in linear operation mode, with a fundamental frequency of 89.6 Hz and a switching frequency

of 5000 Hz. The machine is working at full power, with the 6 modules operative, delivering a total power of 5MW. The average winding temperature is 135 ºC. First, the harmonic content of voltages and currents is compared, and then the loss model is matched to with the information of the machine losses. Fig 5-13 shows both the measured and the simulated voltage harmonic composition. As observed, the results of match with the ones obtained with the model.

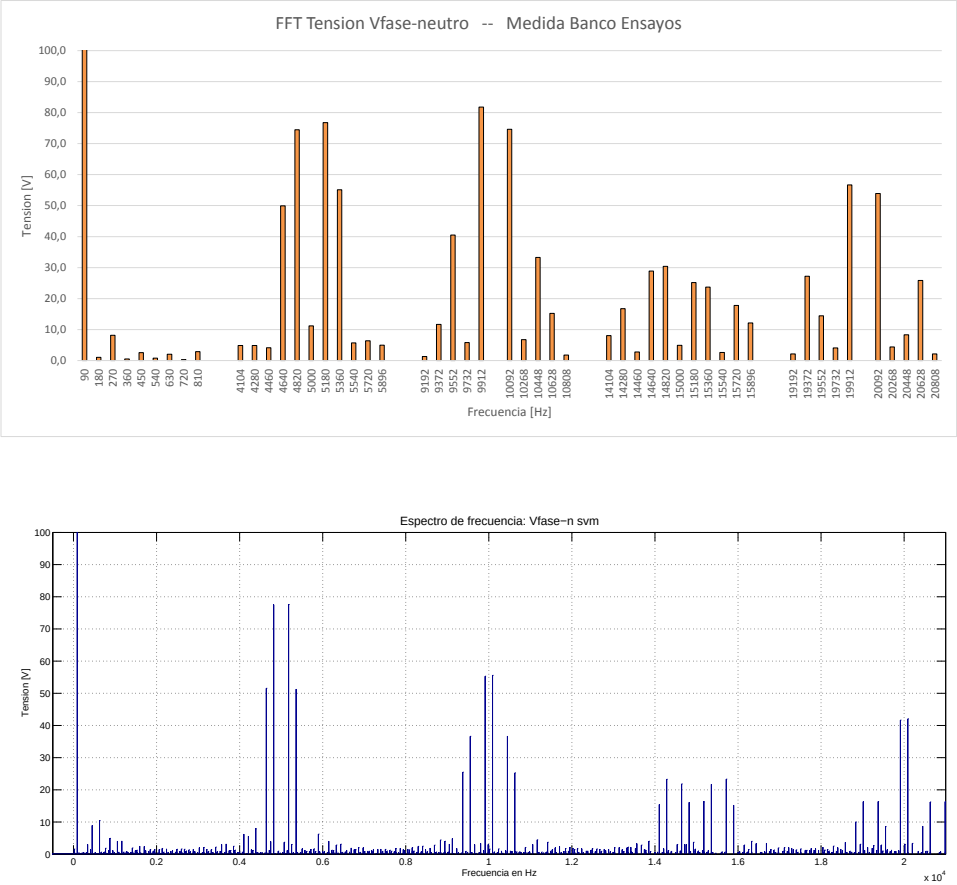

Figure 5-13: FFT of V_{ph-n}. Experimental (top) and simulated (bottom) data values.

The measured and simulated current harmonic spectrum is given in 5-14, showing a deviation in the amplitude of the lateral bands of the harmonics around the multiples of the switching frequencies. These deviations can occur due to multiple reasons:

- Eventhough the LCR filter has been modeled, some differences may exist with experimental set up.

- Control in the model is done in open loop.
- Inductance decrease with increasing frequency has not been modeled.

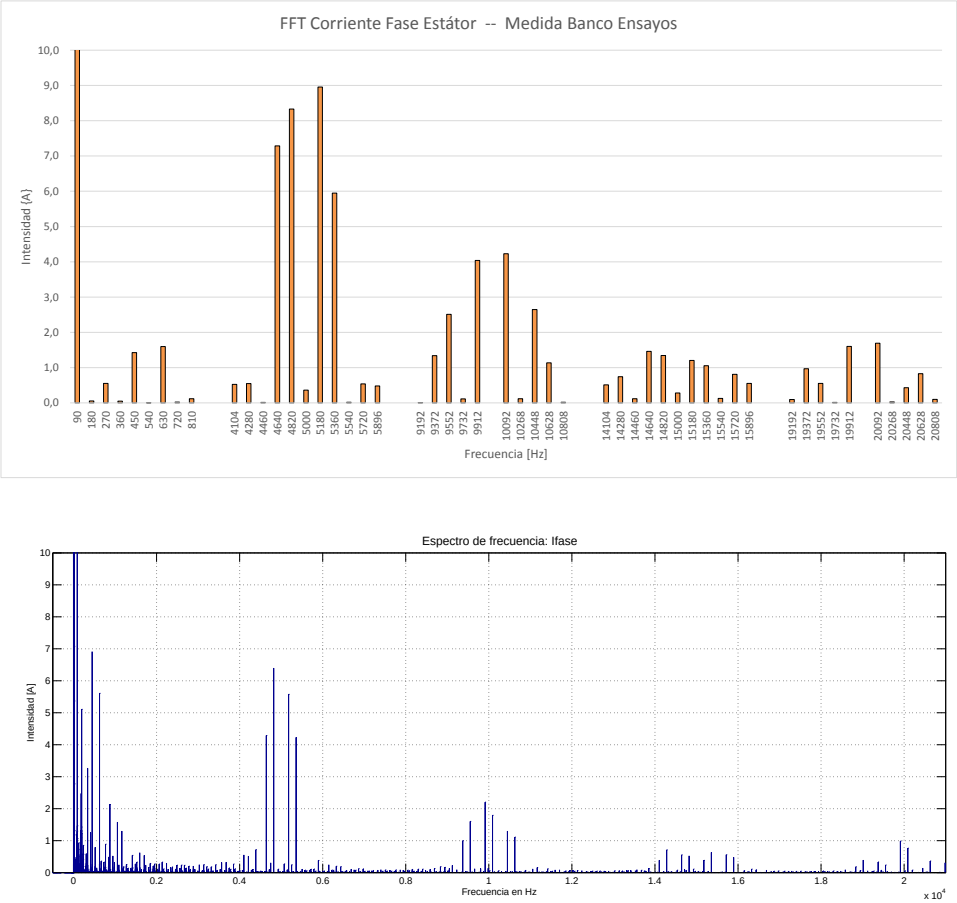

Figure 5-14: FFT of I_{ph}. Experimental (top) and simulated (bottom) data values.

However, the results shown in Fig. 5-14 show the similitude of the model with respect to the measured currents.

Finally, a decomposition of the losses in the frequency spectrum is performed, and the data is plotted against the experimental measurements in fig. 5-15. A final breakdown of the losses is presented in Table 5.2.

Even though the additional losses produced by the increment of the AC resistance at the fundamental frequency and at the rest of frequencies do not present an exact match with the results simulated, the total losses present a good match (error<2%), which makes this model valid, after all the considerations that have been commented,

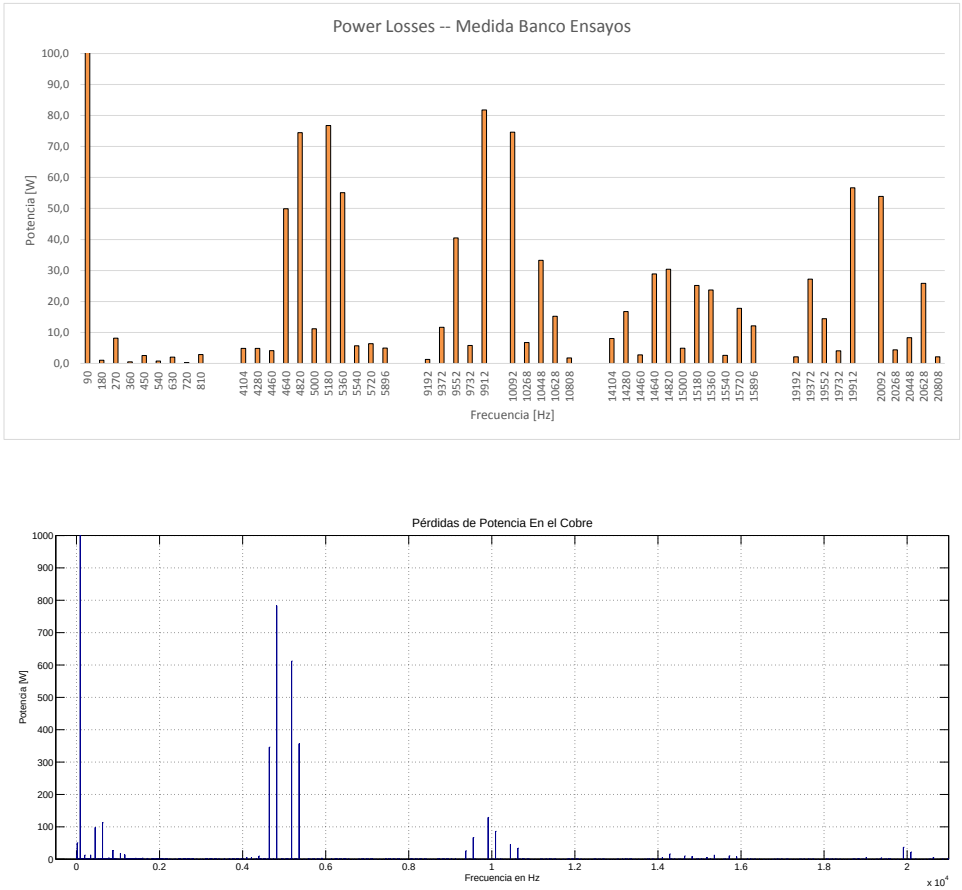

Figure 5-15: Frequency decomposition of the stator power losses. Experimental (top) and simulated (bottom) data values.

for the estimation of the additional copper losses of this machine.

Table 5.2: Harmonic composition of the machine losses.

	P_{dc} [kW]	P_{ac}, f_n [kW]	P_{ac}, rest of f [kW]	P total [kW]
A-type test bench	21.58	24.3	<8	53.88
A-type simulation	21.55	27.6	3.3	52.45

Chapter 6

Conclusions and Future Developments

6.1 Conclusions

This work has evinced the industrial but also academic need of developing a tool for the calculation of additional copper losses in PMSM. The existing mathematical models for such task have been compiled, and a computer tool solution has been provided. This tool will be actually used in future designs of PMSM, as it has been found to be somewhat useful both for the calculation of the machine copper losses, but also to predict the electrical behavior of the machine when interacting with the inverter.

An exhaustive analysis of the harmonic components in the voltage at the output of the inverter has been done, covering the two-level H-bridge three phase inverters using SPWM and SVPWM modulation techniques as well as the three-level NPC inverter using SPWM. Once the voltages have been analyzed, the steady-state model of the machine is used in order to get the current harmonics. These are very similar to the voltage harmonics; in fact, the only difference lies in their amplitude.

However, in order to calculate the losses in the stator windings, it becomes mandatory a precise knowledge about the machine geometry: specially about the winding type, the wires used, the connections scheme, the number of systems... this has been

only possible as a member of the Electric Machine Department from Gamesa Electric. When calculating additional losses in the machines, the literature that can be found related to this topic is not wide spread; in fact, very little references have been found for this purpose. However, these references exhibit general equations in which small changes in the winding geometry that have consequences in the additional losses are not considered, making the research process obscured as the calculations are refined. Thus, based on empirical measurements in the machines, some correction factors are necessary, to try to cover in a general way as many types of IPMSM machine winding designs as possible.

Nevertheless, the model developed is valid for the type A Generator, scope of the study, and is a good starting point for its extension not only to other PMSM stators, but also to other full-converter fed asynchronous machines stator losses, or the rotor losses of the DFIG family. However, this task would require a representative number of data sets of machines that has been impossible to collect.

6.2 Future Developments

This work has developed the tool to calculate and show the additional losses in an specific type of IPMSM, focusing on the copper losses coming from the modulation of inverter; however, this modulation also affects the iron losses and the magnetic behavior of the machine. Therefore, an interesting continuation of this project would be to study the iron losses in this machines, and to define the effects that the switching patterns have on the *additional iron losses* of the machine.

However, the process requires a co-simulation between Finite Element Method software and an electric transient simulator like Simulink, in order to be able to introduce the switched signal to a FEM magnetic model of the machine. This solution already exists, one of the possibilities would be to use FLUX program from CEDRAT coupled with Simulink from Matlab, but the computational requirements would be huge.

Another interesting way of continuing this work would be to extend the study to

Discontinuous PWM modulation techniques.

Finally, as already commented, this model could be generalized not only to all PMSM, if experimental data to contrast with was available in a representative number of machines, but also to asynchronous and DFIG machines.

6.3 Quality Report

I would like to take this opportunity and thank again the Machine Design Department staff, from Gamesa Electric, for the kind support and the valuable knowledge provided during my internship and the realization of this Master Thesis. They provided all the information that I needed, and spent all the necessary time until my model / tool was ready, helping with doubts and guiding my initiation to the industry environment.

However, I would like to point out that the department where I spent my internship time, could not appreciate the skills and knowledge acquired by me during the Master; in other words, I had to change my mind from the electronic converters used in Wind Power Generation, to the electrical and mechanical needs in the design and manufacture of the Electric Machines. This issue has given me a great perspective of the overall system, and has opened several doors to my future career, but also was a little disappointment not to be able to share my knowledge achieved during this 18 last months in the EECPS Master.

Finally, I will remark the benefits of this agreement between Gamesa Electric and University of Oviedo, which has given me the change to do a qualitative leap on the industry environment, and to clarify what I want to do in my near future, and also to help the company with my little contribution; I wish that this agreement lasts for long and that other students like me can enjoy the benefits of doing the internship at this company, as I think both parts can be greatly satisfied and take advantage of each other.

Chapter 7

Work done at Gamesa Electric

While developing my Master Thesis in Gamesa Electric, I gained a different perspective as the one obtained in the EECPS Master, as I was with the Electric Machine Department. All the requirements needed to build a machine, from the first electric design, all the corrections, the mechanical considerations, the manufacturing process and techniques, the constraints and the abilities of each of the individuals that take part in the construction of the final product contributed to an awesome experience.

I was able to join a new work group, and to be beneficiary of their knowledge, both in electrical and mechanical aspects of the construction and analysis of PMSM machines, as well as asynchronous/induction motors, DFIG generators and salient-pole synchronous machines (for hydro-generation). I also contributed to the company by doing my Master Thesis Project as an internal project for the company; I hope that it is somewhat useful and that it can be used in the following designs of the IPMSM, as well as other mechanical and electrical calculations for the company that had nothing to do with the project, but were very instructive for me in the sense that I pushed my mind in as many directions as I could.

I would strongly encourage the incoming students of the EECPS Master to push hard and try to get an internship position at a company; as the overall change from University to industry is huge, and it is good to acquire the perspective of the industry needs, their rules, their environment and their way of working.

Appendix A

AC winding diagrams

As a complement to this Master Thesis, provided that the winding geometry has a direct impact on the additional copper losses, three different winding diagrams are included as an explicative example of the concentrated, wave, and lap windings. The schemes represent a 360º projection of the inner surface of the stator, showing the layout of every coil of the set of windings. Depending on the type of connection of the stator (delta, star) a phase output cable or a neutral cable will be available at the connections side of the scheme. The process of design includes to check all paths and connections for each phase, and to verify that the poles are correctly conformed and that the sense of rotation is the correct one. Once verified, this diagrams suffice to carry out the manufacturing process of the stator windings of a machine.

Note: the G10x modular winding connections scheme is not included due to copyright restrictions.

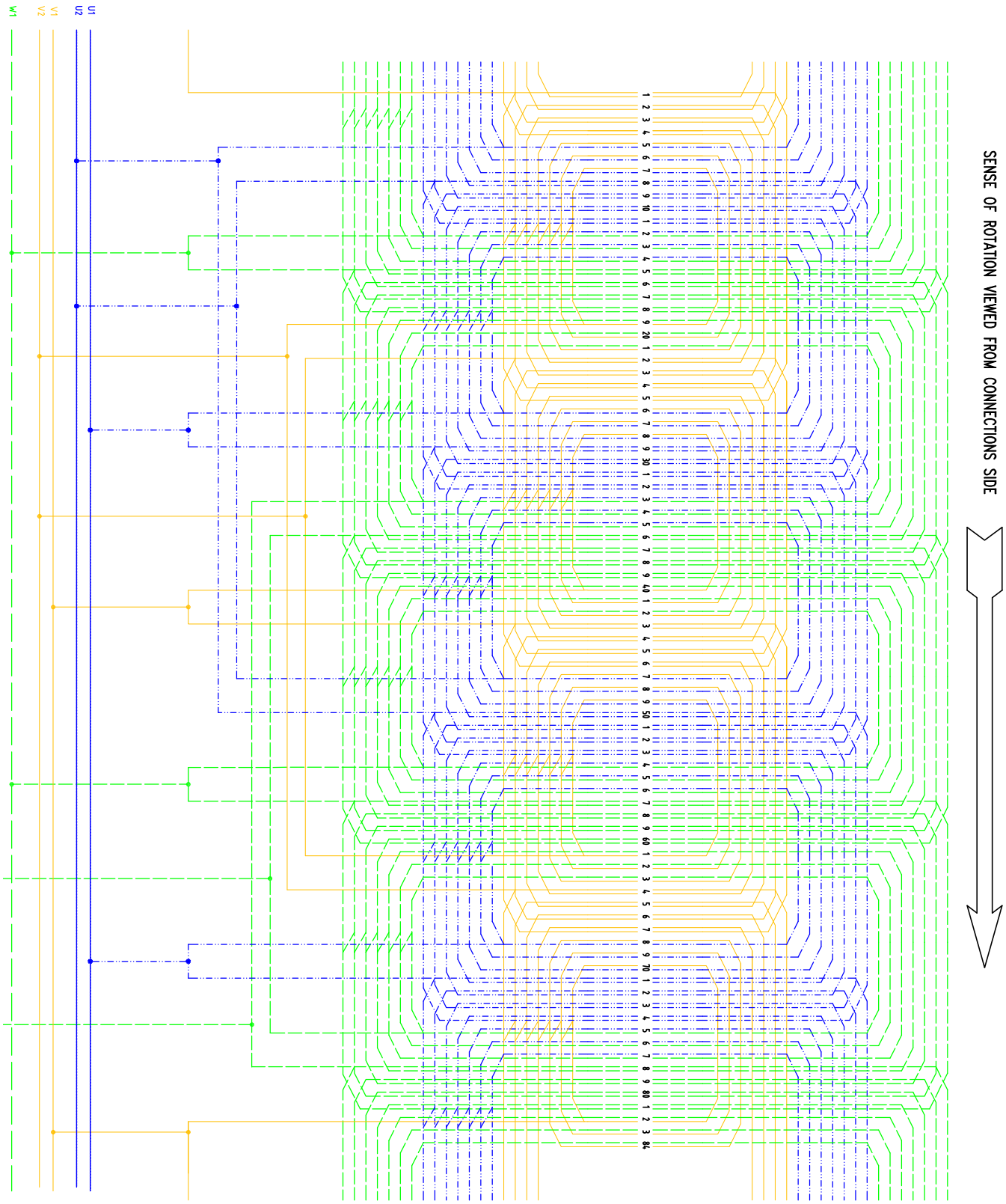

Figure A-1: Concentric winding diagram of a 4 pole, 3 phase stator with delta connection. Q=84, G=12, q=7, $Y_k = 18$, a=4.

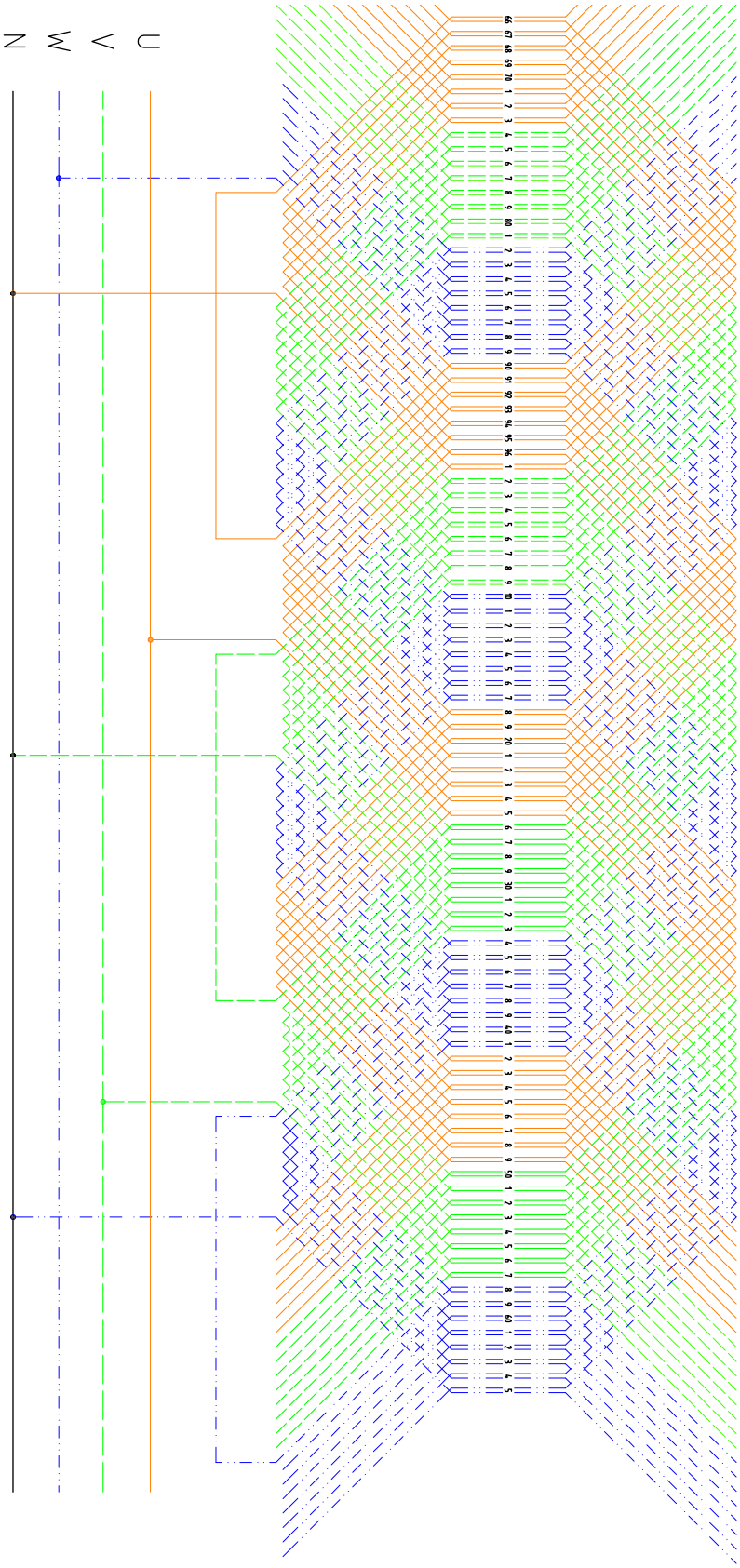

Figure A-2: Distributed wave winding diagram of a 4 pole, 3 phase stator with star connection. Q=96, G=12, q=8, $Y_d = 24$, $Y_k = 23$, a=1.

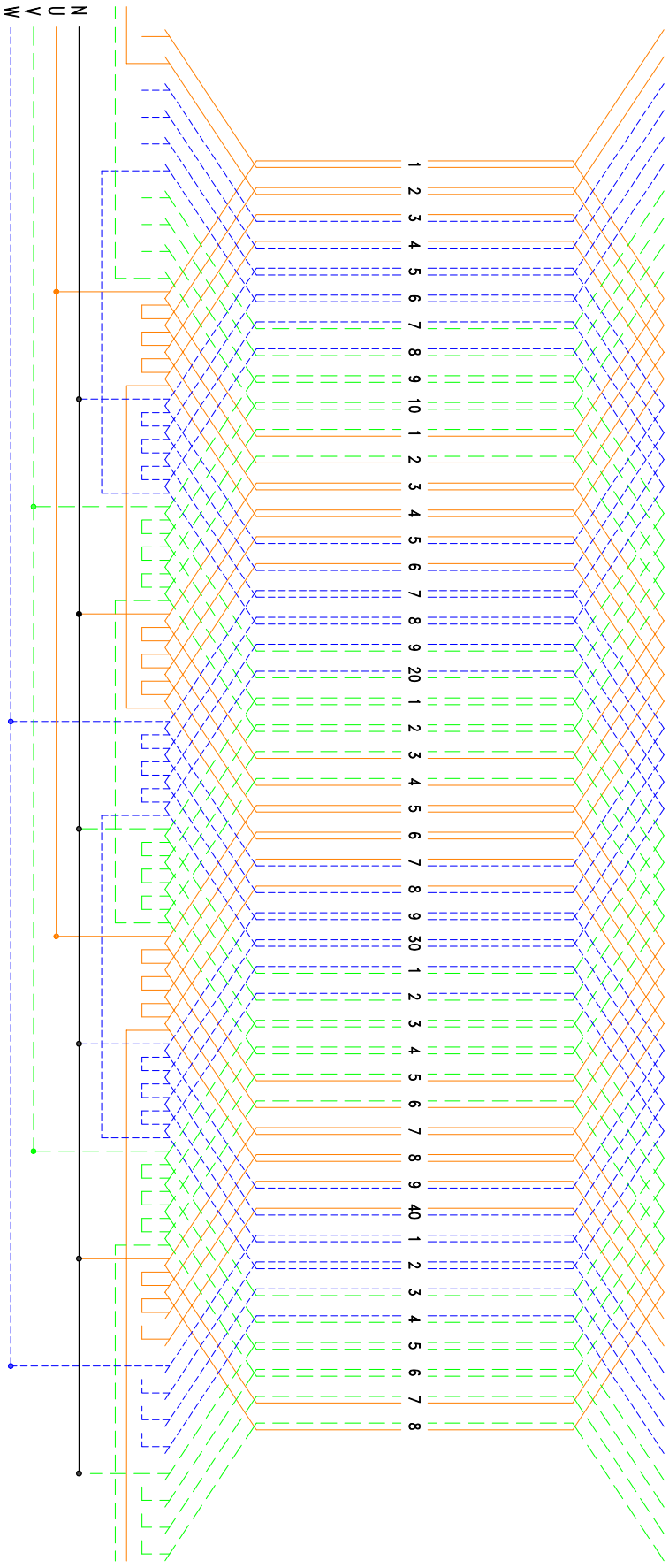

Figure A-3: Distributed lap winding diagram of a 4 pole, 3 phase stator with star connection. Q=48, G=12, q=4, $Y_{\%}$= 10, a=2.

Bibliography

[1] Winding factors and joule losses of permanent magnet machines with concentrated windings.

[2] Lloyd H. Dixon. Eddy current losses in transformer windings and circuit wiring.

[3] P.L. Dowell. Effects of eddy currents in transformer windings. *Proceedings of the Institution of Electrical Engineers*, 113(8):1387–1394, August 1966.

[4] AB. Field. Eddy currents in large slot-wound conductors. *American Institute of Electrical Engineers, Proceedings of the*, 24(7):659–686, July 1905.

[5] D. Grahame Holmes and Thomas A. Lipo. *Pulse Width Modulation for Power Converters: Principles and Practice*. John Wiley & Sons, October 2003.

[6] D.G. Holmes. The significance of zero space vector placement for carrier-based PWM schemes. *IEEE Transactions on Industry Applications*, 32(5):1122–1129, September 1996.

[7] J. Holtz. Pulsewidth modulation for electronic power conversion. *Proceedings of the IEEE*, 82(8):1194–1214, August 1994.

[8] A Iqbal, A Lamine, I Ashraf, and Mohibullah. Matlab/simulink model of space vector PWM for three-phase voltage source inverter. In *Universities Power Engineering Conference, 2006. UPEC '06. Proceedings of the 41st International*, volume 3, pages 1096–1100, September 2006.

[9] Jiri Lammeraner & Milos Stafl. *Eddy Currents*.

[10] G. Joksimović and A. Binder. Additional no-load losses in inverter-fed high-speed cage induction motors. *Electrical Engineering*, 86(2):105–116, January 2004.

[11] K. G. King. A three phase transistor class-b inverter with sine wave output and high efficiency - buscar con google. 1974.

[12] Hans Kleinrath. *Stromrichtergespeiste Drehfeldmaschinen*. Springer, 1980.

[13] Waldo V. Lyon. Heat losses in the conductors of alternating-current machines. *American Institute of Electrical Engineers, Transactions of the*, XL:1361–1409, January 1921.

[14] Juan Corrales Martin. Calculo Industrial De Maquinas Electricas (t. 1).

[15] Jesús Fraile Mora. *Máquinas eléctricas*. McGraw-Hill Interamericana de España S.L., February 2008.

[16] Jesús Rapp Ocariz. *Teoría y cálculo de los bobinados eléctricos*. l'autor, 1987.

[17] Juha Pyrhonen, Tapani Jokinen, and Valeria Hrabovcova. *Design of Rotating Electrical Machines*. John Wiley & Sons, February 2009.

[18] A Reatti and M.K. Kazimierczuk. Comparison of various methods for calculating the AC resistance of inductors. *IEEE Transactions on Magnetics*, 38(3):1512–1518, May 2002.

[19] H.W. Van der Broeck, H.-C. Skudelny, and G.V. Stanke. Analysis and realization of a pulsewidth modulator based on voltage space vectors. *IEEE Transactions on Industry Applications*, 24(1):142–150, January 1988.

[20] Keliang Zhou and Danwei Wang. Relationship between space-vector modulation and three-phase carrier-based PWM: a comprehensive analysis [three-phase inverters]. *IEEE Transactions on Industrial Electronics*, 49(1):186–196, February 2002.